A circulating subset of iNKT cells mediates antitumor and antiviral immunity

AUTHOR(S):

Cui, Guangwei; Shimba, Akihiro; Jin, Jianshi; Ogawa, Taisaku; Muramoto, Yukiko; Miyachi, Hitoshi; Abe, Shinya; ... Noda, Takeshi; Shiroguchi, Katsuyuki; Ikuta, Koichi

CITATION:

Cui, Guangwei ...[et al]. A circulating subset of iNKT cells mediates antitumor and antiviral immunity. Science Immunology 2022, 7(76): eabj8760.

ISSUE DATE:

2022-10

URL:

http://hdl.handle.net/2433/276888

Title:

A Circulating Subset of iNKT Cells Mediates Antitumor and Antiviral Immunity

Authors:

Guangwei Cui[1,*], Akihiro Shimba[1,2], Jianshi Jin[3], Taisaku Ogawa[3], Yukiko Muramoto[4], Hitoshi Miyachi[5], Shinya Abe[1], Takuma Asahi[1,6], Shizue Tani-ichi[1,2], Johannes M. Dijkstra[7], Yayoi Iwamoto[8], Kirill Kryukov[9,10], Yuanbo Zhu[1], Daichi Takami[1,11], Takahiro Hara[1], Satsuki Kitano[5], Yan Xu[12], Hajime Morita[8], Moyu Zhang[8], Lynn Zreka[8], Keishi Miyata[13], Takashi Kanaya[14], Shinya Okumura[15], Takashi Ito[15], Etsuro Hatano[15], Yoshimasa Takahashi[16], Hiroshi Watarai[17], Yuichi Oike[13], Tadashi Imanishi[9], Hiroshi Ohno[14], Toshiaki Ohteki[18], Nagahiro Minato[12], Masato Kubo[19,20], Georg A. Holländer[21,22,23], Hideki Ueno[8], Takeshi Noda[4], Katsuyuki Shiroguchi[3] & Koichi Ikuta[1,*]

Affiliations:

[1]Laboratory of Immune Regulation, Department of Virus Research, Institute for Life and Medical Sciences, Kyoto University, Kyoto, Japan.

[2]Department of Human Health Sciences, Graduate School of Medicine, Kyoto University, Kyoto, Japan.

[3]Laboratory for Prediction of Cell Systems Dynamics, RIKEN Center for Biosystems Dynamics Research (BDR), Osaka, Japan.

[4]Laboratory of Ultrastructural Virology, Department of Virus Research, Institute for Life and Medical Sciences, Kyoto University, Kyoto, Japan.

[5]Reproductive Engineering Team, Institute for Life and Medical Sciences, Kyoto University,

Kyoto, Japan.

[6]Graduate School of Medicine, Kyoto University, Kyoto, Japan.

[7]Institute for Comprehensive Medical Science, Fujita Health University, Aichi, Japan.

[8]Department of Immunology, Graduate School of Medicine, Kyoto University, Kyoto, Japan.

[9]Biomedical Informatics Laboratory, Department of Molecular Life Science, Tokai University, Kanagawa, Japan.

[10]Biological Networks Laboratory, Department of Informatics, National Institute of Genetics, Shizuoka, Japan

[11]Graduate School of Pharmaceutical Science, Kyoto University, Kyoto, Japan.

[12]Medical Innovation Center, Graduate School of Medicine, Kyoto University, Kyoto, Japan.

[13]Department of Molecular Genetics, Graduate School of Medical Sciences, Kumamoto University, Kumamoto, Japan.

[14]Laboratory for Intestinal Ecosystem, RIKEN Center for Integrative Medical Sciences (IMS), Yokohama, Japan.

[15]Division of Hepato-Biliary-Pancreatic Surgery and Transplantation, Department of Surgery, Graduate School of Medicine, Kyoto University, Kyoto, Japan.

[16]Research Center for Drug and Vaccine Development, National Institute of Infectious Diseases, Tokyo, Japan.

[17]Department of Immunology and Stem Cell Biology, Faculty of Medicine, Institute of Medical, Pharmaceutical and Health Sciences, Kanazawa University, Ishikawa, Japan.

[18]Department of Biodefense Research, Medical Research Institute, Tokyo Medical and Dental University, Tokyo, Japan.

[19]Laboratory for Cytokine Regulation, RIKEN Center for Integrative Medical Sciences (IMS),

Yokohama, Japan.

[20]Division of Molecular Pathology, Research Institute for Biomedical Science, Tokyo University of Science, Chiba, Japan.

[21]Weatherall Institute of Molecular Medicine, University of Oxford, Oxford, United Kingdom.

[22]Pediatric Immunology, Department of Biomedicine, University of Basel and University Children's Hospital Basel, Basel, Switzerland.

[23]Department of Biosystems Science and Engineering, ETH Zurich, Basel, Switzerland.

*Corresponding authors: ikuta.koichi.6c@kyoto-u.ac.jp (K.I.); sai1122@hotmail.com (G.C.).

Abstract:

Invariant natural killer T (iNKT) cells are a group of innate-like T lymphocytes that recognize lipid antigens. They are supposed to be tissue-resident and important for systemic and local immune regulation. To investigate the heterogeneity of iNKT cells, we re-characterized iNKT cells in the thymus and peripheral tissues. iNKT cells in the thymus were divided into three subpopulations by the expression of the natural killer cell receptor CD244 and the chemokine receptor CXCR6 and designated as C0 ($CD244^{-}CXCR6^{-}$), C1 ($CD244^{-}CXCR6^{+}$), or C2 ($CD244^{+}CXCR6^{+}$) iNKT cells. The development and maturation of C2 iNKT cells from C0 iNKT cells strictly depended on IL-15 produced by thymic epithelial cells. C2 iNKT cells expressed high levels of IFN-γ and granzymes and exhibited more NK cell-like features, whereas C1 iNKT cells showed more T cell-like characteristics. C2 iNKT cells were influenced by the microbiome and aging and suppressed the expression of the autoimmune regulator AIRE in the thymus. In peripheral tissues, C2 iNKT cells were circulating, which was distinct from conventional tissue-resident C1 iNKT cells. Functionally, C2 iNKT cells protected mice from the tumor metastasis of melanoma cells by enhancing anti-tumor immunity and promoted anti-viral immune responses against influenza virus infection. Furthermore, we identified human $CD244^{+}CXCR6^{+}$ iNKT cells with high cytotoxic properties as a counterpart of mouse C2 iNKT cells. Thus, this study reveals a circulating subset of iNKT cells with NK cell-like properties distinct from conventional tissue-resident iNKT cells.

One Sentence Summary:

A circulating subset of iNKT cells with NK cell-like properties drives effective anti-tumor and anti-viral immunity.

INTRODUCTION

Invariant natural killer T (iNKT) cells are a group of innate-like T lymphocytes and have diverse functions straddling innate and adaptive immune responses. Importantly, they are placed at the frontline for protection against cancer and infection, and are involved in chronic inflammation. iNKT cells express invariant T cell receptors (TCRs) and recognize lipid antigens presented on CD1d, a non-polymorphic MHC class I-like molecule (*1*, *2*). Upon stimulation by a potent synthetic antigen, α-galactosylceramide (α-GalCer), or inflammatory cytokines, iNKT cells are rapidly activated and produce large amounts of the cytokines IFN-γ and IL-4, which enhance innate immune responses by activating antigen-presenting cells (APCs) and NK cells (*3*, *4*). Activated iNKT cells induce the maturation of APCs via CD40 ligand and augment adaptive immune responses. They also express Fas ligand and TNF-related apoptosis-inducing ligand (TRAIL) and exert cytolytic functions (*2*). Notably, iNKT cells are considered to be non-circulating, tissue-resident cells. The regulation and function of iNKT cells differ between tissues, which is important for tissue homeostasis and immunity (*5*, *6*). However, how iNKT cells acquire their heterogeneous homeostasis and function remains unclear.

Like conventional T cells, iNKT cells develop in the thymus from $CD4^+CD8^+$ double positive (DP) thymocytes through positive selection (*1*, *7-11*). Murine iNKT cells are separated into four stages according to their intrathymic development. Stage 0 iNKT cell precursors (defined as $CD24^{high}CD44^-NK1.1^-$) differentiate from DP thymocytes, then downregulate CD24 and become stage 1 immature iNKT cells ($CD24^{low}CD44^-NK1.1^-$). Subsequently, stage 1 iNKT cells change into stage 2 immature iNKT cells ($CD24^{low}CD44^+NK1.1^-$) and finally differentiate into stage 3 mature iNKT cells ($CD24^{low}CD44^+NK1.1^+$). iNKT cells can also be classified into NKT1, NKT2, and NKT17 based on the expression of transcription factors and cytokines,

similar to helper T cell subsets (*4*). Besides their similarity with conventional T cells, iNKT cells express a variety of NK cell receptors and the cytotoxic molecules perforin and granzymes. However, how iNKT cells acquire NK-like or innate-like features during development needs to be clarified.

Interleukin-15 (IL-15) is a pivotal cytokine for the differentiation, maintenance, and response of immune cells (*12, 13*). It is constitutively produced by stromal and hematopoietic cells in various organs, and its local expression is enhanced during inflammation and immune responses (*14, 15*). IL-15 exerts its functions on lymphocytes expressing IL-2/15Rβ chain and common γ-chain through trans-presentation with its high affinity receptor IL-15Rα. Previous studies in mice lacking IL-15 or IL-15Rα demonstrate that the IL-15 signal plays an essential role in the development and homeostasis of iNKT cells (*16, 17*). We have identified and characterized IL-15-producing cells in each organ by using IL-15-CFP knock-in reporter mice (*15*). However, it remains unclear whether different IL-15 niches play a role in the heterogeneity of tissue iNKT cells.

To address these questions, we characterized iNKT cells in a series of mice bearing cell type-specific IL-15 deletion. We identified an unrecognized iNKT cell population that depended on IL-15 in the thymus and expressed both NK cell receptor CD244 (also known as 2B4) and chemokine receptor CXCR6. $CD244^{+}CXCR6^{+}$ iNKT cells were circulating in peripheral tissues, displayed more NK cell-like features, suppressed tumor dissemination, and enhanced anti-viral immune responses, whereas $CD244^{-}CXCR6^{+}$ conventional iNKT cells were tissue-resident and exhibited more T cell-like properties. Furthermore, we also identified $CD244^{+}CXCR6^{+}$ iNKT cells that exhibited high cytotoxic properties in people. Thus, this study identifies two subsets of

iNKT cells, one circulating and the other tissue-resident, with distinct development and functions in immunity.

RESULTS

An iNKT cell subset produces high levels of IFN-γ in the thymus at steady state

The majority of thymic iNKT cells are NK1.1^{+}CD44^{+} mature cells (*1, 18, 19*). Herein, we identified an iNKT cell subpopulation that expressed high levels of the natural killer cell receptor CD244 (also known as 2B4) and chemokine receptor CXCR6 in the mature fraction of iNKT cells. We designated the CD244^{+}CXCR6^{+} double positive (DP) iNKT cells as C2 (because expressing both CD244 and CXCR6) iNKT cells, CD244^{-}CXCR6^{+} single positive (SP) iNKT as C1 iNKT cells and CD244^{-}CXCR6^{-} double negative iNKT as C0 iNKT cells. The C2 iNKT cells made up 10-20% of mature iNKT cells in the thymus (Fig. 1A) and constantly produced IFN-γ even at steady state, whereas C1 iNKT cells and C0 iNKT cells lacked this expression (Fig. 1, B and C). In addition, the expression of CD244 and CXCR6 was unchanged, but IFN-γ production was enhanced, in C1 and C2 iNKT cells by stimulation with PMA and ionomycin (fig. S1A). The transcription factor PLZF, which is required for the determination of iNKT cell lineages but whose expression decreases with maturation (*20*), was downregulated in C1 and C2 iNKT cells compared to C0 iNKT cells (Fig. 1D and fig. S1B).

iNKT cells are classified into three functionally distinct subsets, IFN-γ-producing NKT1, IL-4-producing NKT2, and IL-17-producing NKT17 cells, with the expression of different transcription factors, T-bet, GATA3, and RORγt, respectively (*4*). The three iNKT cell subsets were also separated by the expression of surface markers: NKT1 cells as IL-17RB^{-}, NKT2 cells as IL-17RB^{+}CD4^{+}, and NKT17 cells as IL-17RB^{+}CD4^{-} (fig. S1C). We found that all C2 iNKT cells were NKT1 cells in C57BL/6 mice, in line with their high IFN-γ expression at steady state (Fig. 1E). We could also detect the CD244^{+}CXCR6^{+} population similar to C2 iNKT cells in mice

on different genetic backgrounds such as BALB/c, although they completely lacked the expression of NK1.1 (fig S1D). Most of these C2-like iNKT cells on a BALB/c background appeared to be in the NKT1 and NKT17 fractions. However, we found that all C2-like iNKT cells in BALB/c mice expressed IFN-γ but not IL-17A upon activation (fig. S1E). These results suggest that C2 iNKT cells are NKT1 cells and may be important for type 1 immunity.

Because iNKT cells comprise $CD4^+$ and $CD4^-$ subpopulations, we next analyzed CD4 expression in C0, C1, and C2 iNKT cells. We found that less than 20% of C2 iNKT cells were $CD4^+$ cells, whereas more than 60% of C0 and C1 iNKT cells were $CD4^+$ cells (Fig. 1F, and fig. S1F), suggesting that C2 iNKT cells are more enriched in the $CD4^-$ subpopulation. C2 iNKT cells expressed higher levels of IFN-γ compared to both the $CD4^+$ and $CD4^-$ fractions of iNKT cells (fig. S1G). However, the expression levels of developmental and functional molecules as well as the production of IFN-γ were comparable in the $CD4^+$ and $CD4^-$ subpopulations of C2 iNKT cells, suggesting that there are almost no phonotypic or functional differences between $CD4^+$ and $CD4^-$ C2 iNKT cells in mice (fig. S1, H and I).

To further characterize thymic C2 iNKT cells, digital RNA sequencing (dRNA-seq) was performed for a comprehensive genomic profile. We identified a distinct cluster of C2 iNKT cells that was clearly separated from other clusters of C0 and C1 iNKT cells in the thymus by principal component analysis (PCA) (Fig. 1G). In contrast, the difference between $CD4^+$ and $CD4^-$ C2 iNKT cells was much smaller than the differences among C2, C1, and C0 iNKT cells (fig. S1J). Genes related to granzymes, chemokines, interferons, integrins, and killer cell lectin-like receptors (KLRs) were highly expressed in C2 iNKT cells (Fig. 1H). Gene enrichment analysis revealed the enhanced expression of genes correlated with cell cytotoxicity and activation in C2 iNKT cells (Fig. 1I). Coincidentally, we found that Klf2, a transcription factor

important for natural killer (NK) cell homeostasis (*21*), was expressed at high levels in C2 iNKT cells compared to C1 iNKT cells (Fig. 1, H and J). In contrast, the expression of genes related to TCR signal strength or T cell activation, such as ICOS, Lef1 and CD5, was higher in C1 iNKT cells (Fig. 1, H and K, and fig. S1K). We then performed PCA using the dRNA-seq data of C0, C1, and C2 iNKT cells combined with CD4 SP T, CD8 SP T, and NK cells (Fig.1L). In addition, PD-1, which is associated with the activation or exhaustion of T cells, showed comparable levels between C1 and C2 iNKT cells (fig. S1L). Furthermore, we found that the frequency of C2 iNKT cells was higher in young mice but lower in aged mice (Fig. 1M). Besides existing in the thymus, C2 iNKT cells were detected in the bone marrow, peripheral blood, and several peripheral tissues, with a higher frequency in mucosal tissues such as the lung and lamina propria of intestine than in the spleen or liver (Fig. 1N). Taken together, these results suggest that C2 iNKT cells exhibit a more NK cell- or innate-like identity, whereas C1 iNKT cells represent a more T cell-like property.

The development and maturation of C2 iNKT cells is dependent on the thymic epithelial IL-15 niche

IL-15, an essential cytokine for iNKT cells, is produced in the thymus by medullary thymic epithelial cells (mTECs), blood vascular endothelial cells (BECs), and myeloid cells (*15*). To elucidate the thymic IL-15 niche for C1 and C2 iNKT cell subsets, we generated and analyzed FoxN1-Cre IL-15 conditional knockout (cKO) mice, which lack IL-15 expression in TECs (fig. S2). Stage 3 mature iNKT cells and NKT1 cells significantly decreased in the thymus of FoxN1-Cre IL-15 cKO mice, whereas other T cells remained unchanged (Fig. 2, A and B, and fig. S3, A and B). The survival and proliferation of thymic iNKT cells were promoted by mTEC-derived

IL-15 (Fig. 2, C and D). Importantly, we found that C2 iNKT cells had disappeared in FoxN1-Cre IL-15 cKO mice, whereas C1 iNKT cells were reduced by half and C0 iNKT cells were unchanged (Fig. 2, E and F). The numbers of C1 and C2 iNKT cells were not recovered in FoxN1-Cre IL-15 cKO mice in the presence of transgenic Bcl-2 expression, which elevates cell survival, whereas C0 iNKT cells significantly increased (fig. S3C). In addition, besides iNKT cells, we also found that γδT1 cells, which is a small population of thymocytes, were modestly decreased in FoxN1-Cre IL-15 cKO mice (fig. S3, D and E), consistent with a recent report (*22*). To exclude any influence from γδT1 cells, we analyzed FoxN1-Cre IL-15 cKO × TCRδ KO mice. We found that the three iNKT cell subsets changed very similarly compared with FoxN1-Cre IL-15 cKO mice (fig. S3F), suggesting that γδT1 cells have minimal, if any, effect on iNKT cells. In addition, some well-known IL-15-dependent lymphocytes such as NK cells, mucosa-associated invariant T (MAIT) cells, and intraepithelial lymphocytes (IELs) were unchanged in FoxN1-Cre IL-15 cKO mice (Fig. 2G and fig. S3, G to K).

To assess the IL-15-dependent development and maturation of C0, C1, and C2 iNKT cells, we differentiated each iNKT cell population ex vivo in the presence or absence of IL-15. Almost all C0 iNKT cells differentiated into either C1 or C2 iNKT cells at equal frequency, and a small fraction of C1 iNKT cells displayed the potential to mature into C2 iNKT cells in the presence of IL-15 (Fig. 2, H and I). The phenotype of C2 iNKT cells remained unchanged after stimulation, indicating that C2 iNKT cells are the most mature subset. In contrast, the development from C0 or C1 iNKT cells into C2 iNKT cells was impaired in the absence of IL-15. This IL-15 dependence was confirmed in vivo, as the administration of IL-15–IL-15Rα complexes (RLI) enhanced the frequency of C2 iNKT cells (Fig. 2J). Furthermore, we performed an intrathymic injection of C0 iNKT cells from CD45.1 mice into CD45.2 recipients. We

observed that C0 iNKT cells differentiated into C1 and C2 iNKT cells in vivo (Fig. 2K). However, stimulation with α-GalCer, a ligand for the TCR of iNKT cells, failed to promote C2 iNKT cells in the absence of IL-15 in FoxN1-Cre IL-15 cKO mice (Fig. 2L). Taken together, these results suggest that the development and maturation of C2 iNKT cell depend on the thymic epithelial IL-15 niche.

C2 iNKT cells are controlled by the trans-presentation of IL-15–IL-15Rα on mTECs

Because IL-15–IL-15Rα trans-presentation controls IL-15 signaling (*13*), we also employed IL-15Rα cKO mice to examine the precise IL-15 signal transduction for C2 iNKT cell development in vivo. Interestingly, C2 iNKT cells were absent in the thymus of FoxN1-Cre IL-15Rα cKO mice, a phenotype similar to FoxN1-Cre IL-15 cKO mice (Fig. 3A), indicating that IL-15–IL-15Rα trans-presentation by mTECs is indispensable for C2 iNKT cell development. Additionally, other T cells and NK cells remained unchanged in FoxN1-Cre IL-15Rα cKO mice (fig. S4A). Although BECs in the thymus expressed high levels of IL-15, a Tie-Cre IL-15 cKO mouse model with bone marrow transplantation elucidated that BEC-derived IL-15 did not affect iNKT cells or other T cells in the thymus (Fig. 3B and fig. S4B). We then asked whether iNKT cell development or maintenance was also promoted by IL-15–IL-15Rα trans-presentation between TECs and myeloid cells, since some myeloid cells such as macrophages and dendritic cells (DCs) express IL-15 and IL-15Rα in the thymus. However, the numbers of iNKT cells and T cells were unchanged in the thymus of LysM-Cre and CD11c-Cre IL-15 cKO mice (Fig. 3, C and D, and fig. S4, C and D). Coincidently, IL-15Rα presented by myeloid cells and thymocytes themselves did not affect iNKT cell development or maintenance in the thymic IL-15 niche (fig.

S4, E to G). Taken together, these results demonstrate that the IL-15–IL-15Rα trans-presentation by mTECs controls C2 iNKT cells in vivo.

C2 iNKT cells are adjacent to mTECs and regulate self-antigen expression for immune tolerance in the thymus

To clarify the spatial relationship between IL-15-producing mTECs and iNKT cells in the thymus, we carried out immunohistochemistry experiments on IL-15-CFP knock-in mice. Many iNKT cells were distributed around IL-15-producing cells in the thymic medulla, and a quantification of contacting thymocytes showed that iNKT cells were more adjacent to IL-15-producing mTECs than CD4 and CD8 SP thymocytes (Fig. 3, E and F, and fig. S5, A and B). Furthermore, we found that C2 iNKT cells constituted approximately 45% of $CD244^{+}TCR\beta^{+}$ cells in the thymus (fig. S5C), and that the majority of these $CD244^{+}TCR\beta^{+}$ cells were adjacent to IL-15-CFP^{+} TECs in the thymic medulla (fig. S5, D and E). Collectively, these results suggest that IL-15-producing mTECs may provide preferable sites for the development and maintenance of C2 iNKT cells.

Because we found that C2 iNKT cells were the major source of IFN-γ in the thymus at steady state (Fig. 3, G and H), we investigated the function of IFN-γ produced by C2 iNKT cells in the thymic epithelial IL-15 niche. The expressions of the autoimmune regulator AIRE, a transcription factor which induces the self-antigen expression in mTECs (*23*), and an AIRE-dependent self-antigen, Ins2, were elevated in mTECs, and $AIRE^{+}$ mTECs appeared to increase in FoxN1-Cre IL-15 cKO mice (Fig. 3, I and J), consistent with a previous report that IFN-γ influences the self-antigen expression by mTECs (*24*). By contrast, the expression of Fezf2, another regulator of self-antigen expression in mTECs, remained unchanged (fig. S5F).

Furthermore, we employed a CD1d1/2 KO mouse line, which lacks iNKT cells, and found that the expression levels of AIRE by mTECs were comparable between FoxN1-Cre IL-15 cKO × CD1d1/2 KO mice and control CD1d1/2 KO mice (Fig. 3K), suggesting that alteration of AIRE expression was iNKT cell-dependent. Overall, C2 iNKT cells express high levels of IFN-γ, which may suppress the expression of AIRE and AIRE-dependent self-antigens in mTECs for immune tolerance.

C2 iNKT cells are influenced by the gut microbiome

The gut microbiome alters with age and may influence iNKT cell homeostasis (*25*). Because thymic C2 iNKT cells were reduced with aging (Fig. 1M), we compared thymic iNKT cells between specific pathogen-free (SPF) and germ-free (GF) conditions. The frequency of thymic C2 iNKT cells in GF mice was lower than in 4-week-old SPF mice (Fig. S6, A and B). However, the frequency of C2 iNKT cells was unchanged by antibiotic treatment in 12-week-old mice (fig. S6C), suggesting that microbiota influence C2 iNKT cells only in younger mice or that the antibiotic treatment did not eliminate the microbiota that impact C2 iNKT cells. Together, these results suggest that the frequency of thymic C2 iNKT cells may be influenced by the gut microbiome.

Heterogeneity of peripheral C1 and C2 iNKT cells

We characterized C1 and C2 iNKT cells in the peripheral tissues of FoxN1-Cre IL-15 cKO mice. Despite C1 iNKT cells being recovered, C2 iNKT cells remained severely reduced in the lung, spleen, peripheral blood, and liver (Fig. 4, A to D and fig. S7A). In addition, we also confirmed that the numbers of C1 and C2 iNKT cells in the lung of FoxN1-Cre IL-15 cKO mice × TCRδ

KO mice changed very similarly as in FoxN1-Cre IL-15 cKO mice (fig. S7B). Although the T cell number in the peripheral tissues of FoxN1-Cre IL-15 cKO mice was comparable to control mice, NK cells in FoxN1-Cre IL-15 cKO mice seemed to slightly increase in the lung and spleen (fig. S7, C to F), unlike in the thymus where NK cells were unchanged (Fig. 2G), suggesting that C2 iNKT cells may negatively influence NK cell maintenance in peripheral tissues at steady state. These results suggest that the thymic epithelial IL-15 niche is important for peripheral C2 iNKT cells and that FoxN1-Cre IL-15 cKO mice are a valuable tool for analyzing the functions of C2 iNKT cells in vivo.

To further investigate the differences between C1 and C2 iNKT cells in the peripheral tissues, we isolated iNKT cells from the lung, where C2 iNKT cells were relatively abundant, and analyzed their gene expression profile by dRNA-seq. Lung C1 and C2 iNKT cells were separated into two distinct clusters by PCA (Fig. 4E). In comparison to C1 iNKT cells, C2 iNKT cells in the lung expressed higher levels of chemokines, granzymes, integrins, and KLRs, but lower levels of Satb1, ICOS and Ly6a, and the expression pattern of these genes was similar to that in the thymus (Fig. 4F and fig. S7G). Furthermore, the transcription factor for NK cell homeostasis, Klf2, was also higher in lung C2 iNKT cells (Fig. 4F). To compare the in vivo distribution, we performed intravascular staining with anti-CD45 antibody. The majority of T and NK cells were present within blood vessels of the lung, whereas C1 iNKT cells were preferentially localized in the lung parenchyma (Fig. 4, G and H). Notably, the frequency of C2 iNKT cells was between these other cell types, indicating that C2 iNKT cells have more transmigration activity between the lung parenchyma and blood vessels. To reveal the dependency on the peripheral IL-15 niche, we analyzed lung C1 and C2 iNKT cells in LysM-Cre and CD11c-Cre IL-15 cKO mice for myeloid cell-derived IL-15 and SPC-Cre IL-15 cKO mice

for pulmonary epithelial cell-derived IL-15. We found that the expansion or maturation of lung C1 iNKT cells partially depended on IL-15 produced by peripheral myeloid cells, whereas C2 iNKT cells in the lung were independent of peripheral IL-15 (Fig. 4, I and J, and fig. S7H). In addition, peripheral IL-15 also contributed to the maintenance of NK cells in the lung (Fig. 4, I and J). Taken together, C2 iNKT cells display more innate-cell like properties than C1 iNKT cells and depend on the thymic epithelial IL-15 niche even in the peripheral tissues, whereas C1 iNKT cells partially depend on the myeloid IL-15 niche in the peripheral tissues.

Distinct cell dynamics of peripheral C1 and C2 iNKT cells

iNKT cells are considered to be non-circulating, tissue-resident cells (*5*, *26*). To further investigate how C1 and C2 iNKT cells are maintained by different IL-15 niches and distributed in distinct manners in the peripheral tissues, we performed parabiosis experiments between CD45.1 and CD45.2 mice to assess the dynamics of C1 and C2 iNKT cells. Notably, we found that C2 iNKT cells circulated in the peripheral tissues such as the lung and spleen, like NK cells but contrary to C1 iNKT cells, which showed significantly higher tissue residency (Fig. 5, A to D, and fig. S8, A and B). Consistent with recent reports that a purinergic receptor, P2X7R, is related to the tissue-residency of lymphocytes and that tissue-resident iNKT cells are preferentially controlled by P2X7R activation (*27*), P2X7R was expressed more in lung C1 iNKT cells than in C2 iNKT cells (Fig. 5, E and F). A similar pattern of iNKT cell residency was observed in the bone marrow (Fig. 5, G and H), whereas C1 and C2 iNKT cell populations mixed almost equally in peripheral blood according to the parabiosis experiments (fig. S8, C and D). In the thymus, all C0, C1, and C2 iNKT cells were tissue-resident (Fig. 5I), consistent with a

previous report that NK1.1$^+$ iNKT cells are retained in the thymus (*18*). The expression levels of P2X7R were similar between C1 and C2 iNKT cell populations in the thymus (Fig. 5, J and K).

Because CXCR6, the receptor for CXCL16, is implicated in the tissue retention of iNKT cells (*28*), we next analyzed CXCR6 KO mice. We found that C1 iNKT cells were significantly reduced in the lungs of CXCR6 KO mice, whereas C2 iNKT cells were unaffected (Fig. 5L). Because C2 iNKT cells expressed higher levels of integrin α1 (CD49a), we administered anti-CD49a blocking antibody into the mice. The number of C2 iNKT cells, but not C1 iNKT cells, was partially reduced in the lung (Fig. 5M). Of note, neither CXCR6 deficiency nor CD49a blocking impaired thymic iNKT cell development or maintenance (fig. S8, E and F). Klf2, a transcription factor highly expressed in C2 iNKT cells, has been reported to regulate T cell trafficking by promoting S1pr1 (*29*). We found that the S1pr1 expression was upregulated in C2 iNKT cells (fig. S8G). Furthermore, the frequency of intravascular C2 iNKT cells was modestly decreased by FTY720 treatment, an antagonist of S1P1, similar to the alteration of intravascular T cells (fig. S8H). Taken together, these results suggest that C2 iNKT cells are a circulating iNKT cell subset and that their retention and migration in peripheral tissues are affected by integrin α1 and S1P1. In contrast, C1 iNKT cells represent a tissue-resident iNKT subset that requires CXCR6 for its tissue residency.

C2 iNKT cells exhibit high cytotoxicity and enhance anti-tumor immunity

Because iNKT cells have potent anti-tumor activity by linking innate and adaptive immunity (*30-32*), we employed a B16-F10 melanoma metastasis model to assess C2 iNKT cell function in anti-tumor immunity. Metastatic nodules in the lung were increased in FoxN1-Cre IL-15 cKO mice as well as FoxN1-Cre IL-15 cKO × TCRδ KO mice when compared to control mice (Fig. 6,

A and B, and fig. S9A), which correlated with a significant decrease of C2 iNKT cells (Fig. 6C and fig. S9B). In addition, NK cells, especially KLRG1^{+} mature NK cells, were fewer, and their proliferation and activation were reduced following the B16-F10 melanoma inoculation in FoxN1-Cre IL-15 cKO mice (Fig. 6, C to E). On the other hand, the numbers of C1 iNKT cells, T cells, and B cells, which are also important for anti-tumor immunity, were unchanged in the lungs of FoxN1-Cre IL-15 cKO mice after the inoculation (Fig. 6C and fig. S9C). Because CD8 T cells and NK cells exert their effector functions in anti-tumor immunity by producing IFN-γ, we analyzed the IFN-γ expression by using IFN-γ-Venus reporter mice. We found that CD8 T cells and NK cells produced comparable levels of IFN-γ between FoxN1-Cre IL-15 cKO mice and control mice after the inoculation of B16-F10 melanoma cells, suggesting that effector functions of CD8 T cells and NK cells may be unchanged in FoxN1-Cre IL-15 cKO mice (fig. S9D). Additionally, there was no difference in the number of metastatic nodules in the lungs of FoxN1-Cre IL-15 cKO × CD1d1/2 KO mice and control CD1d1/2 KO mice (Fig. 6F). Collectively, these data suggest that C2 iNKT cells are involved in anti-tumor immunity.

Next, to assess the direct cytotoxicity of C2 iNKT cells, we checked the expression of IFN-γ and the cytotoxic molecules such as granzyme B, perforin, and TRAIL, which mediate anti-tumor immunity. C2 iNKT cells produced higher levels of IFN-γ and granzyme B than C1 iNKT cells after B16-F10 melanoma inoculation (Fig. 6, G and H). Notably, C2 iNKT cells expressed extremely high levels of IFN-γ, like NK cells (Fig. 6G), whereas the levels were of CD4^{+} and CD4^{-} C2 iNKT cells and were similar (fig. S9E). Upon co-culture with B16-F10 melanoma cells after TCR and IL-15 stimulation, C2 iNKT cells expressed higher levels of granzyme B, perforin, and TRAIL than C1 iNKT cells (Fig. 6, I and J, and fig. S9F). Moreover, a

tumor inhibition assay showed that C2 iNKT cells had significantly higher cytotoxic activity than C1 iNKT cells against B16-F10 melanoma cells (Fig. 6K).

To confirm the function of C2 iNKT cells in anti-tumor immunity, we adoptively transferred C2 iNKT cells from CD45.1 mice into CD45.2 FoxN1-Cre IL-15 cKO recipient mice one day after the inoculation of B16-F10 melanoma cells (fig. S9G). Metastatic nodules in the lung were significantly decreased in mice with C2 iNKT cell transfer (Fig. 6L). The number of NK cells, especially KLRG1^{+} mature NK cells, increased after the adoptive transfer of C2 iNKT cells, whereas the numbers of T cells and B cells were unchanged (Fig. 6, M and N, and fig. S9H). However, the IFN-γ expression by relevant cells was unaltered after the adoptive transfer of C2 iNKT cells (Fig. 6O). α-GalCer injection in mice activates whole iNKT cells and enhances anti-tumor immunity (*33*). We found that tumor metastases were also reduced in FoxN1-Cre IL-15 cKO mice after stimulation with α-GalCer, maybe because the strong activation of C1 iNKT cells compensated for the lack of C2 iNKT cells (fig. S9I). Moreover, we found that the tumor cells suppressed the development and maturation of C2 iNKT cells from C0 and C1 iNKT cells in ex vivo culture even in the presence of IL-15 (fig. S9, J and K). These results suggest that C2 iNKT cells seems to be inhibited within the tumor microenvironment, whereas the thymic IL-15 niche may provide a uniquely preferable site for them. Taken together, these findings suggest that C2 iNKT cells are a highly effective tumor-suppressing iNKT cell subset and that they enhance anti-tumor immunity against cancer metastasis in the lung. The function of C2 iNKT cells in anti-tumor immunity may be ascribed to their high cytotoxic activity against tumor cells and their supporting activity for the proliferation and maturation of NK cells.

C2 iNKT cells promote the anti-viral immune response against influenza virus infection

Although the consequences of IL-15 expression and iNKT cells in the control of pulmonary virus infection have been well discussed (*3*, *4*), the role of circulating iNKT cells in virus infection is unknown. To address this question, FoxN1-Cre IL-15 cKO and control mice were infected intranasally with a 0.5 LD_{50} (50% lethal dose) of influenza A virus (IAV). In accordance with the importance of IFN-γ production in anti-viral immunity mediated by lymphocytes, we found that C2 iNKT cells highly expressed IFN-γ in response to IAV infection (Fig. 7A). In line with an impaired virus clearance (Fig. 7B), C2 iNKT cells were significantly decreased in FoxN1-Cre IL-15 cKO mice, whereas the number of C1 iNKT cells was unchanged compared to control mice after IAV inoculation (Fig. 7C). Consistently, IAV-infected FoxN1-Cre IL-15 cKO mice exhibited a reduced frequency and absolute number of IAV-specific CD8 T cells compared to IAV-infected control mice (Fig. 7, D and E). The number of NK cells moderately decreased, whereas the numbers of CD4 and CD8 T cells were unchanged (Fig. 7F). Furthermore, virus clearance was unchanged between FoxN1-Cre IL-15 cKO × CD1d1/2 KO mice and control CD1d1/2 KO mice, suggesting that C2 iNKT cells were involved in anti-viral immunity (Fig. 7G). In addition, as $CD11b^{+}Gr1^{+}$ myeloid-derived suppressor cells (MDSCs) effectively suppress anti-viral immunity (*34*), we next analyzed MDSCs and found that the frequency and number of MDSCs increased in IAV-infected FoxN1-Cre IL-15 cKO mice (Fig. 7H and fig. S10A), whereas the numbers of other myeloid cells such as DCs were unchanged (fig. S10, B and C).

To confirm the function of C2 iNKT cells in anti-viral immunity, we adoptively transferred C2 iNKT cells from CD45.1 mice into CD45.2 FoxN1-Cre IL-15 cKO recipient mice and infected the mice with IAV on the same day. The virus clearance was significantly accelerated in FoxN1-Cre IL-15 cKO mice following the C2 iNKT cell transfer (Fig. 7I). The

numbers of C1 iNKT cells, NK cells, and CD8 T cells, especially IAV-specific CD8 T cells, were elevated in FoxN1-Cre IL-15 cKO recipient mice after the adoptive transfer of C2 iNKT cells, whereas MDSCs slightly decreased, but not significantly, and CD4 T cells were unchanged compared to FoxN1-Cre IL-15 cKO mice (Fig. 7, J to M, and fig. S10D). Furthermore, IFN-γ production in C1 iNKT cells was upregulated, whereas IFN-γ production in other cells was not altered after adoptive transfer of C2 iNKT cells (Fig. 7N), suggesting that C2 iNKT cells may promote the effector function of C1 iNKT cells in anti-viral immunity. By contrast, when we infected the mice with a lethal dose (2 LD_{50}) of IAV, the body weight loss became much milder, and the survival rate was higher in FoxN1-Cre IL-15 cKO mice than control mice (fig. S10, E and F), suggesting that an attenuated anti-viral immune response may result in a delay of virus clearance, leading to sustained inflammation, tissue damage, and increased mortality in FoxN1-Cre IL-15 cKO mice. Collectively, these results suggest that circulating C2 iNKT cells enhance the immune response against IAV infection.

Human C2 iNKT cells exhibit high cytotoxicity like mouse C2 iNKT cells

Since CD244 and CXCR6 are expressed in human iNKT cells in peripheral blood (*35*) and the expression levels correlate with disease progression in human immunodeficiency virus (HIV) patients (*36*), we further investigated iNKT cells in human samples. $CD244^{+}CXCR6^{+}$ and $CD244^{-}CXCR6^{+}$ iNKT cell subpopulations corresponding to mouse C2 and C1 iNKT cells, respectively, were detectable in human peripheral blood and liver perfusates (Fig. 8A and fig. S11A). Notably, all human C2 iNKT cells were $CD4^{-}$ cells (Fig. 8B). We also found that the frequency of human C2 iNKT cells was higher in young donors (18 to 32 years old) and lower in aged donors (52 to 56 years old) (Fig. 8, A and C), suggesting the possibility that it is due to the

higher thymic dependency of C2 iNKT cells. Human C2 iNKT cells also highly expressed IFN-γ compared to human C1 iNKT cells after stimulation, similar to mouse C2 iNKT cells, whereas the production of IL-17 was undetectable (Fig. 8D and fig. S11B).

Finally, we analyzed gene expression of human C2 and C1 iNKT cells by dRNA-seq. We found that human C2 and C1 iNKT cells were separated into two distinct clusters by PCA (Fig. 8E). Gene expression profiling revealed that human C2 iNKT cells expressed high levels of genes related to granzymes, granulysin, and perforin for iNKT-cell mediated effector functions and KLRs, like mouse C2 iNKT cells (Fig. 8F). Gene enrichment analysis also showed an enhanced expression of genes correlated with cell cytotoxicity and activation in human C2 iNKT cells (Fig. 8G). Furthermore, we checked whether developmental and functional molecules were highly expressed on the cell surface of human C2 iNKT cells by flow cytometry. Human C2 iNKT cells expressed higher levels of CD161, CD94, and CCR5, and lower levels of ICOS, compared to C1 iNKT cells (Fig. 8H and fig. S11C). Taken together, these data suggest that human C2 iNKT cells exhibit high cytotoxicity and activity important for type 1 immunity, similar to mouse C2 iNKT cells.

DISCUSSION

iNKT cells are a group of innate-like T lymphocytes and have been classified by their maturational stages or lineage diversification with specific transcription factors (*1*, *2*). They are considered to be non-circulating, tissue-resident cells (*5*, *6*, *26*). In this study, however, we identified circulating iNKT cells (C2 iNKT cells) in mice that were distinct from conventional tissue-resident iNKT cells (C1 iNKT cells). We defined C2 iNKT cells as $CD244^{+}CXCR6^{+}$ DP iNKT cells in NKT1 cells. In concert with the notion that conventional iNKT cells contribute to local immunity such as tissue-specific homeostasis and protection, C1 iNKT cells exhibited tissue-resident properties and probably play the same role. In contrast to tissue-resident lymphocytes, circulating lymphocytes actively survey the body to encounter antigens and evoke systemic immune responses. In this sense, C2 iNKT cells with circulating properties can probably sense detrimental insults such as metastatic tumor cells or invading microorganisms and orchestrate systemic immunity by their high cytotoxicity and by activating relevant immune cells. C2 iNKT cells depended on the thymic IL-15 niche for their development and maturation, whereas C1 iNKT cells were probably maintained by a distinct peripheral IL-15 niche. Furthermore, we also identified $CD244^{+}CXCR6^{+}$ human C2 iNKT cells, a human counterpart of mouse C2 iNKT cells, that exhibited high cytotoxicity. Thus, we propose a layered structure of iNKT cells composed of tissue resident C1 and circulating C2 iNKT subsets. This structure is analogous to that of group 1 innate lymphoid cells (ILCs) with tissue resident ILCs and conventional circulating NK cells. These two subsets of iNKT cells together provide diverse systemic and tissue-specific immune regulations.

We found that C2 iNKT cells were a highly IFN-γ-producing iNKT cell subset in the thymus at steady state. C2 iNKT cells seemed to interact with IL-15-producing mTECs and

received trans-presented IL-15-IL-15Rα for their development and maturation. Of interest, we found that C2 iNKT cells were the major source of IFN-γ in the thymus. Similar to IFN-γ-deficient mice (*24*), FoxN1-Cre IL-15 cKO mice, which lack C2 iNKT cells, exhibited an elevated expression of AIRE, suggesting a crosstalk between C2 iNKT cells and mTECs. It is known that the crosstalk between thymocytes and mTECs is crucial for the development of the thymic medulla (*37*, *38*), and we found that iNKT cells in the medulla were adjacent to mTECs. Thus, IL-15-producing mTECs may provide a preferred site for C2 iNKT cell development and maturation from C0 iNKT cells, and, conversely, C2 iNKT cells expressing IFN-γ might regulate immune tolerance through the expression of AIRE-dependent tissue-specific antigens.

Despite C1 iNKT cells being recovered, C2 iNKT cells remained severely reduced in peripheral tissues such as the lung, spleen, peripheral blood, and liver. These results suggested that C1 iNKT cells may have undergone expansion or maturation in peripheral tissues, whereas the development and maturation of C2 iNKT cells by IL-15 was limited to the thymic medulla. Yet, there remains another possibility that the recovery in the peripheral tissues may be due to the different emigration rates between C2 and C1 iNKT cells.

In the lungs, C2 iNKT cells were associated with the lung parenchyma by integrin α1, similar to memory CD8 T cells (*39*), whereas C1 iNKT cells required the chemokine receptor CXCR6, as previously reported for iNKT cell localization (*28*). C2 iNKT cells in the peripheral tissues showed a similar gene expression pattern to those in the thymus, with more NK cell- or innate cell-like properties. In accordance with their circulating properties, C2 iNKT cells expressed S1PR1 at higher levels, suggesting that C2 iNKT cells may recirculate in a S1P1-dependent manner (*29*). Besides the higher expression of genes related to cell activity, mobility, and cytotoxicity, C2 iNKT cells also highly expressed several NK cell receptors including

CD244 (2B4) and killer cell lectin-like receptors, which have both positive and negative functions (*40*). In contrast to the marked decrease of C2 iNKT cells in mice with IL-15 deficiency in the thymus, NK cells, another IL-15-dependent innate-like lymphocyte cell type, were slightly increased in the peripheral tissues. Because C2 iNKT cells were reduced in the peripheral tissues and did not depend on peripheral IL-15, we speculate that C2 iNKT cells may have suppressive effects on peripheral NK cells at steady state, however, the precise mechanism needs to be investigated further.

iNKT cells are influenced by the microbiota in intestines and involved in inflammatory bowel diseases, and iNKT cells from GF mice are hypo-responsive compared with those from SPF mice (*25*). Another study showed that the number of iNKT cells increases after the monocolonization of neonatal GF mice with *Bacteroides fragilis* (*41*). We found a reduction of thymic C2 in parallel with aging, and that C2 iNKT cells were decreased in 4-week-old GF mice. Because the gut microbiome alters with weaning, these data suggest that dietary changes may have influenced C2 iNKT cell development by the microbiota. However, the frequency of C2 iNKT cells was unchanged in antibiotic-treated 12-week-old mice, maybe due to the high antibiotics resistance of *Bacteroides fragilis (42)*. Our data also may explain the notion that alterations of the gut microbiome in young mice have more profound effects on iNKT cells than in aged mice.

In contrast to the influence of the microbiota, iNKT cells provide protection against various pathogens such as bacteria and viruses (*43*). iNKT cells play an important role in host defense at the early phase of infection through the recognition of microbial glycolipids. C2 iNKT cells, which were highly cytotoxic and highly express IFN-γ, may contribute to this process more efficiently with their circulating properties. In addition, peripheral C2 iNKT cells highly

expressed TLR2 and IL-1β, which are involved in immune responses against influenza virus (*44*). They also secreted abundantly chemokines such as CCL2, CCL5, and CXCL2, which are related to immune cell recruitment and elevated in influenza virus infection (*45*). Although viral infections may not induce the synthesis of lipid antigens, iNKT cells undergo activation, show protective effects in the lung and liver, and expand virus-specific memory CD8 T cells (*34*). Notably, we found that virus clearance was impaired in FoxN1-Cre IL-15 cKO mice after infection with a 0.5 LD_{50} dose of IAV, with a concomitant decrease of IAV-specific CD8 T and NK cells and increase of MDSCs, whereas the adoptive transfer of C2 iNKT cells rescued the attenuated immune response. These results suggest that C2 iNKT cells enhance anti-viral immunity against lung IAV infection. It is possible that the expansion and activation of IAV-specific CD8 T cells and NK cells may be due to both direct activation by C2 iNKT cells and the indirect effect of MDSC suppression by C2 iNKT cells. Because iNKT cells reduce IAV-induced MDSCs (*34*) and apolipoprotein E (ApoE) restricts MDSC maintenance (*46*), C2 iNKT cells probably function as an effective MDSCs- suppressing iNKT subset in IAV infection by their high expression of ApoE (Fig. 4F). Furthermore, it is reported that microbiota regulate immune defenses against IVA infection (*47*), and our results suggest that C2 iNKT cells may be involved in this process. Nevertheless, similar to the results of IL-15 knockout mice (*48*), FoxN1-Cre IL-15 cKO mice showed milder body weight loss and decreased mortality risk after a lethal dose of IAV infection, suggesting that circulating C2 iNKT cells may also be a key regulator for the pathogenesis of IAV-induced acute lung injury, which leads to the progression of symptoms and mortality.

Besides their direct effector functions, iNKT cells activate NK cells and CTLs by IFN-γ and induce the maturation of DCs via cognate TCR-CD1d interactions (*2*). The lung metastasis

of B16-F10 melanoma cells was exacerbated in mice in the absence of C2 iNKT cells, and the adoptive transfer of C2 iNKT cells into FoxN1-Cre IL-15 cKO mice rescued the impairment. Thus, these results suggest that besides tissue-resident C1 iNKT cells, circulating C2 iNKT cells also contribute to iNKT cell-mediated antitumor immunity. Consistent with the high expression of cytotoxic molecules, such as IFN-γ, granzyme B, perforin, and TRAIL, C2 iNKT cells had direct tumor inhibitory activity. Our data also suggest the possibility that C2 iNKT cells may promote NK cell activation and maturation in the B16-F10 melanoma metastasis model. Taken together, circulating C2 iNKT cells serve as a highly effective tumor-suppressing iNKT cell subset in vivo. Because conventional tissue-resident iNKT cells may trigger a tissue-repair program that in turn may promote tumor progression (*5*), the rapid and direct suppression of cancer metastasis by C2 INKT cells may be important for anti-tumor immunity. We propose that C2 iNKT cells circulate in the peripheral tissues, contributing to cancer immunosurveillance. Furthermore, because of their high mobility and effector functions, C2 iNKT cells may become a useful tool to trigger local immune responses against cancers.

It is reported that human $CD4^+$ and $CD4^-$ iNKT cells in peripheral blood have distinct features. Human $CD4^-$ iNKT cells express genes associated with the activation of effector functions and cytolysis, which resembles NK cells with Th1 cytokine expression (*35, 49*). In this study, we identified human C2 iNKT cells as human $CD4^-$ iNKT cells with high cell activation and expression of cytotoxic molecules, such as granzymes, granulysin, and perforin, related to iNKT cell-mediated effector functions in anti-tumor and anti-viral immunity. In addition, CCR5, a chemokine receptor important for human T cell trafficking (*50*), was highly expressed in human C2 iNKT cells. A functional enrichment analysis showed that genes enhanced in human C2 iNKT cells may be involved in the SARS-CoV-2 signaling pathway, and it is also reported

that the expression of CD244 in human iNKT cells is correlated with the disease progression of HIV patients (*36*). Thus, the precise roles of human C2 iNKT cells in anti-viral or anti-tumor immunity need future investigations.

In this study, we identified a circulating iNKT cell subset that enhanced anti-tumor and anti-viral immune responses. These cells were distinct from the conventional tissue-resident iNKT cell subset. Our findings lead to the novel idea of a layered structure of iNKT cells with distinct development, dynamics, and functions. Furthermore, they may help advance iNKT cell-targeted immunotherapies against cancers and infections.

MATERIALS AND METHODS

Study design

The aim of this study was to identify and characterize the developmental and functional heterogeneity of circulating and tissue-resident iNKT cells. We performed multimodal analysis with a series of IL-15 reporter mouse and conditional knock-out mouse models, and human samples. Parabiosis was used to classify circulating and tissue-resident iNKT cells. B16-F10 melanoma lung metastasis and influenza A virus (IAV) infection models were used to investigate the function of circulating iNKT cells. The sample size of all the experiments was determined on the basis of our previous studies and prior experiments that were sufficient for statistical analysis and on the consideration of animal welfare. The number of independent experiments is indicated in the figure legends. The mouse experiments were performed unblinded, as mice of different genotypes were identified and kept track of.

Mice and generation of IL-15-floxed mice

One- to 16-week-old male or female IL-15-floxed (generated in this study), IL-15-CFP knock-in (*15*), IFN-γ-Venus reporter (*51*), FoxN1-Cre (*52*), Tie2-Cre (*53*), CD4-Cre (*54*), CD11c-Cre (*55*), LysM-Cre (*56*), CXCR6-GFP/GFP (KO) (*57*), CD1d1/2 knock-out (KO) (*58*), TCRδ KO (*59*), SPC-Cre mice (*60*), and IL-15Rα-floxed mice on a C57BL/6 background were used. For more details, see the Supplementary Materials. All mice were maintained under specific pathogen-free (SPF) conditions at the Experimental Research Center for Infectious Diseases, Institute for Life and Medical Sciences, Kyoto University. All procedures were carried out under Sevoflurane

anesthesia to minimize animal suffering. All mouse protocols were approved by the Animal Experimentation Committee of the Institute for Life and Medical Sciences, Kyoto University.

Human samples

The human peripheral blood samples were collected from 18- to 52-year-old male or female donors who provided informed consent for the study, which was approved by the Institutional Review Board (IRB) at Kyoto University (IRB number: G1212). The human peripheral blood samples from 20- to 56-year old male or female donors were obtained from HemaCare Corp. (Northridge, CA). The human liver perfusates samples were collected from donors who provided informed consent for the study, which was approved by the IRB at Kyoto University (IRB number: G1240).

Cell isolation

Lymphocytes from the indicated tissues were prepared as described previously (*61*, *62*). After perfusion with PBS, the lung was minced with scissors and incubated at 37℃ for 1 hour in RPMI 1640 medium containing 10% FBS, 1 mg/mL collagenase D and 50 μg/mL Dnase (Roche). Digested tissue was suspended and passed through a 40-μm strainer (Greiner Bio-One). Leukocytes were separated by centrifugation through 30% Percoll. The isolation of mTECs was performed as described previously (*15*).

Flow cytometry

Cells were prepared from the indicated organs and surface-stained for 20 minutes at 4°C in PBS containing 0.2% BSA and 0.05% NaN_3 with fluorescent dye- or biotin-conjugated antibodies.

Detailed antibody information is shown in Supplementary table S1. Biotinylated monoclonal antibodies were detected with PE- or Brilliant Violet 421-conjugated streptavidin (Thermo Fisher Scientific). PBS57-loaded mouse and human CD1d tetramer or PBS57-unloaded control, and 5-OP-RU-loaded MR1 tetramer were kindly provided by the NIH Tetramer Core Facility. For more details, see the Supplementary Materials.

Cell culture

iNKT cells were sorted using a FACSAria II cell sorter (BD Biosciences) into a tube with RPMI 1640 medium containing 10% FBS, 50 μM 2-mercaptethanol and 10 mM HEPES (pH7.4). For iNKT cell differentiation or maturation, each iNKT cell subset was cultured with 2 μg/ml plate-bound anti-CD3 antibody (145-2C11) with or without 50 ng/mL IL-15 and with or without 1×10^4 B16-F10 melanoma cells at 37℃ in 5% CO_2. After 3 days, all cells were stained with the relevant antibodies for flow cytometry. For the expression of cytotoxic molecules in iNKT cells, lung bulk lymphocytes were cultured with 2 μg/mL plate-bound anti-CD3 antibody, 100 ng/mL IL-15 and 1×10^4 B16-F10 melanoma cells for 12 hours.

Immunohistochemistry

IL-15-CFP knock-in mice were used (*15*), and PBS-57-loaded CD1d tetramer or PBS-57-unloaded control (NIH Tetramer Core Facility) immunofluorescence was performed as described previously (*63*). For more details, see the Supplementary Materials.

Digital RNA-seq and data analysis

Mouse iNKT cells were freshly isolated from the thymus and lungs of C57BL/6 mice. Human iNKT cells were isolated from peripheral blood. Two hundred C1 or C2 iNKT cells were sorted into a tube using a FACS Aria II. Digital RNA-sequencing (dRNA-seq) (*64*, *65*) was performed as described previously (*66*). Differential gene expression and principal component analysis (PCA) were performed using rlog-normalized dRNA-seq data by DESeq2 (*67*), and 95% confidence ellipses for each group are shown in the plot of PCA. Heat maps were drawn on the gene counts, which were normalized by the total counts of all genes using R package ggplots2. To identify genes differentially expressed, $\log_2$ fold changes were calculated between C1 and C2 iNKT cells. Genes were considered differentially expressed when they had $\log_2$ fold changes of ≥ 1 or ≤ -1, and p values ≤ 0.01. Gene enrichment analysis was performed using Metascape (*68*).

Parabiosis

Female 8-week-old congenic CD45.1 and CD45.2 congenic C57BL/6J mice were surgically connected in parabiosis (*69*). Lateral skin from the elbow to knee in each mouse was sutured, the forelimbs and hindlimbs were tied together, and the skin incisions were closed using surgical adhesive. After surgery, the mice were maintained on water containing antibiotics for about 2 weeks to prevent infection and analyzed 60 days later. Partner-derived cells in both parabionts (CD45.1 and CD45.2) were analyzed as independent data points.

Intrathymic injection

Intrathymic injection was performed as previously reported (*18*). For more details, see the Supplementary Materials.

In vivo stimulation of iNKT cells

Mice were administered with 1 μg/mouse α-galactosylceramide (α-Gal) or with IL-15/IL-15Rα complex (RLI). For more details, see the Supplementary Materials.

Integrin α1 blockade

Functional blocking hamster anti-mouse CD49a antibody (Ha31/8) (BD Biosciences) and isotype-matched control antibody (Ha4/8) were used for integrin α1 (CD49a) blocking experiments as described previously (*70*). For each experiment, wild-type mice were administered 150 μg/mouse blocking antibody or isotype-matched control by intravenous (i.v.) injection every two days and analyzed 6 days after the first antibody administration.

Adoptive transfer of C2 iNKT cells

Adoptive transfer experiments were performed as previously reported (*71*). C2 iNKT cells were isolated from the thymus of CD45.1 WT mice and cultured for 1 day with 2 μg/mL plate-bound anti-CD3 antibody (145-2C11) and 50 ng/mL IL-15 for expansion. Approximately 1×10^5 C2 iNKT cells from CD45.1 mice were transferred into CD45.2 FonN1-Cre IL-15 cKO recipients or CD45.2 FoxN1-Cre IL-15 cKO × IFN-γ-Venus reporter mice by i.v. injection. The mice were intravenously inoculated with B16-F10 melanoma cells one day before the transfer or intranasally infected with IAV (PR8) on the same day.

B16-F10 melanoma lung metastasis

The B16-F10 melanoma cell line was cultured in high glucose-containing Dulbecco's modified Eagle's medium (DMEM) supplemented with 10% FBS, 100 U/mL penicillin, 100 μg/mL

streptomycin and 2 mmol/L L-glutamine. For the lung metastasis assay, a single cell suspension of B16-F10 cell was prepared in PBS, and 4×10^4 cells were injected intravenously into recipient mice. The lungs were harvested, tumor nodules were counted on day 14, and lymphocytes were isolated and analyzed.

Tumor inhibition assay

The ex vivo tumor inhibition assay was performed according to a previously report (*72*) with minor modifications. For more details, see the Supplementary Materials.

Intravascular staining

The intravascular staining of CD45 and FTY720 treatment was described previously (*73*, *74*). For more details, see the Supplementary Materials.

Influenza A virus (IAV) infection

The influenza A virus (IAV) used in this study was A/Puerto Rico/8/34 (PR8; H1N1). For IAV infection, 6–8-week-old male or female mice were intranasally administered 50 μL PBS containing 0.5 or 2 LD_{50} dose of IAV/Puerto Rico/8/34 (IAV/PR8, H1N1). For the flow cytometry analysis, mice were sacrificed at day 7 post-infection, and immune cells were isolated from the whole lung. To assess virus-specific CD8 T cells, BV421-conjugated H-$2D^b$ IAV/PR8 $NP_{366\text{-}374}$ tetramer-ASNENMETM, kindly provided by NIH Tetramer Core Facility, was used. For virus titrations, a 50% tissue culture infectious dose ($TCID_{50}$) assay was performed. The lung from mice 4 days post infection was homogenized with 4 volumes of PBS and assayed for virus infectivity on MDCK cells for the cytopathic effect with a 10-fold dilution series. Mice were

monitored daily for body weight loss and survival until death occurred or euthanasia was performed during a period of 14 days. Mice that lost 20% of their body weight were considered to have reached humane endpoints and were euthanized within a day according to the animal experiment protocol.

Real-time RT-PCR

Total RNA was extracted from the sorted cells and reverse-transcribed using random primers. cDNA was analyzed by real-time RT-PCR using SYBR Green PCR Master Mix (Qiagen). For more details, see the Supplementary Materials.

Bone marrow transplantation

Tie2-Cre IL-15 cKO host mice were irradiated and injected with 5×10^5 bone marrow cells. For more details, see the Supplementary Materials.

Antibiotic treatment

Mice 8 weeks of age were orally administered with an antibiotics (ABX) cocktail (1 g/L ampicillin, 0.5 g/L vancomycin, 1 g/L metronidazole, and 1 g/L neomycin) (Sigma) in drinking water. Mice were analyzed at 4 weeks of treatment.

Statistical analysis

All statistical analyses were performed using GraphPad Prism 7 or 8 software. All data are presented as means ± SD or ± SEM. Comparisons between two samples were performed using an unpaired two-tailed Student's *t*-test or unpaired *t*-test with Welch's correction. For multiple

group comparisons, one-way or two-way ANOVA analyses with a multiple-comparison test were used. **, $p < 0.01$; *, $p < 0.05$; n.s., not significant.

Acknowledgments:

We thank Dr. T. Honjo for providing the B16-F10 cell lines, Drs. J. Takeda, K. Yusa, and G. Kondoh for providing the KY1.1 ES line and targeting system, N. Iwasaki for help in preparing the human samples, and K. Fukuhara and R. Yamamoto for help in performing dRNA-seq.

Funding:

This study was supported by Japan Society for the Promotion of Science (JSPS) KAKENHI Grants 19K16687 and 17K15721 (G.C.), 16H05172 and 20H03501 (K.I.), and 18H05411 (K.S.); Research grants from the Takeda Science Foundation (G.C.), as well as Shimizu Foundation for Immunology and Neuroscience grant (G.C.), and by JST Core Research for Evolutional Science and Technology, the Grant for Joint Research Project of the Institute of Medical Science (T.N), and Joint Usage Research Center program of the Institute for Life and Medical Sciences, Kyoto University.

Author contributions:

G.C. and K.I. designed the research and wrote the manuscript. G.C., A.S., J.J., T.O., Y.M., H.M., S.A., T.A., S.T., Y.Z., and K.S. performed the experiments and analyses. H.M., J.M.D., Y.I., K.K., D.T., T.H., S.K., Y.X., H.M., M.Z., L.Z., K.M., T.K., S.O., T.I., E.H., Y.T., H.W., Y.O., T.I., H.O., T.O., N.M., M.K., G.A.H., H.U., T.N., and K.S. provided some important materials, methods, and advice.

Competing interests:

The authors declare no competing interests.

Data and materials availability:

All data needed to evaluate the conclusions in the paper are present in the paper or the Supplementary Materials. The gene expression data of dRNA-seq have been deposited into the Gene Expression Omnibus (GEO) public data set with accession number GSE 150813, GSE 206553 and GSE 206627.

SUPPLEMENTARY MATERIALS

Supplementary Materials and Methods

Figs. S1 to S10

REFERENCES AND NOTES

1. A. Bendelac, P. B. Savage, L. Teyton, The biology of NKT cells. *Annu. Rev. Immunol.* **25**, 297-336 (2007).
2. P. J. Brennan, M. Brigl, M. B. Brenner, Invariant natural killer T cells: an innate activation scheme linked to diverse effector functions. *Nat. Rev. Immunol.* **13**, 101-117 (2013).
3. S. Fujii, K. Shimizu, M. Kronenberg, R. M. Steinman, Prolonged IFN-γ-producing NKT response induced with α-galactosylceramide-loaded DCs. *Nat. Immunol.* **3**, 867-874 (2002).
4. Y. J. Lee, K. L. Holzapfel, J. F. Zhu, S. C. Jameson, K. A. Hogquist, Steady-state production of IL-4 modulates immunity in mouse strains and is determined by lineage diversity of iNKT cells. *Nat. Immunol.* **14**, 1146-1154 (2013).
5. C. M. Crosby, M. Kronenberg, Tissue-specific functions of invariant natural killer T cells. *Nat. Rev. Immunol.* **18**, 559-574 (2018).
6. X. Fan, A. Y. Rudensky, Hallmarks of tissue-resident lymphocytes. *Cell* **164**, 1198-1211 (2016).
7. K. Benlagha, T. Kyin, A. Beavis, L. Teyton, A. Bendelac, A thymic precursor to the NK T cell lineage. *Science* **296**, 553-555 (2002).
8. A. Bendelac, Positive selection of mouse $NK1^+$ T cells by CD1-expressing cortical thymocytes. *J. Exp. Med.* **182**, 2091-2096 (1995).
9. T. Egawa, G. Eberl, I. Taniuchi, K. Benlagha, F. Geissmann, L. Hennighausen, A. Bendelac, D. R. Littman, Genetic evidence supporting selection of the Vα14i NKT cell lineage from double-positive thymocyte precursors. *Immunity* **22**, 705-716 (2005).

10. J. S. Bezbradica, T. Hill, A. K. Stanic, L. Van Kaer, S. Joyce, Commitment toward the natural T (iNKT) cell lineage occurs at the $CD4^{+}8^{+}$ stage of thymic ontogeny. *Proc. Natl. Acad. Sci. U.S.A.* **102**, 5114-5119 (2005).

11. L. Gapin, J. L. Matsuda, C. D. Surh, M. Kronenberg, NKT cells derive from double-positive thymocytes that are positively selected by CD1d. *Nat. Immunol.* **2**, 971-978 (2001).

12. M. K. Kennedy, M. Glaccum, S. N. Brown, E. A. Butz, J. L. Viney, M. Embers, N. Matsuki, K. Charrier, L. Sedger, C. R. Willis, K. Brasel, P. J. Morrissey, K. Stocking, J. C. L. Schuh, S. Joyce, J. J. Peschon, Reversible defects in natural killer and memory CD8 T cell lineages in interleukin 15-deficient mice. *J. Exp. Med.* **191**, 771-780 (2000).

13. A. Ma, R. Koka, P. Burkett, Diverse functions of IL-2, IL-15, and IL-7 in lymphoid homeostasis. *Annu. Rev. Immunol.* **24**, 657-679 (2006).

14. S. L. Colpitts, S. W. Stonier, T. A. Stoklasek, S. H. Root, H. L. Aguila, K. S. Schluns, L. Lefrancois, Transcriptional regulation of IL-15 expression during hematopoiesis. *J. Immunol.* **191**, 3017-3024 (2013).

15. G. W. Cui, T. Hara, S. Simmons, K. Wagatsuma, A. Abe, H. Miyachi, S. Kitano, M. Ishii, S. Tani-ichi, K. Ikuta, Characterization of the IL-15 niche in primary and secondary lymphoid organs in vivo. *Proc. Natl. Acad. Sci. U.S.A.* **111**, 1915-1920 (2014).

16. L. E. Gordy, J. S. Bezbradica, A. I. Flyak, C. T. Spencer, A. Dunkle, J. C. Sun, A. K. Stanic, M. R. Boothby, Y. W. He, Z. M. Zhao, L. Van Kaer, S. Joyce, IL-15 regulates homeostasis and terminal maturation of NKT cells. *J. Immunol.* **187**, 6335-6345 (2011).

17. E. Mortier, R. Advincula, L. Kim, S. Chmura, J. Barrera, B. Reizis, B. A. Malynn, A. Ma, Macrophage- and dendritic-cell-derived interleukin-15 receptor α supports homeostasis

of distinct CD8$^+$ T cell subsets. *Immunity* **31**, 811-822 (2009).

18. S. P. Berzins, F. W. McNab, C. M. Jones, M. J. Smyth, D. I. Godfrey, Long-term retention of mature NK1.1$^+$ NKT cells in the thymus. *J. Immunol.* **176**, 4059-4065 (2006).

19. F. W. McNab, D. G. Pellicci, K. Field, G. Besra, M. J. Smyth, D. I. Godfrey, S. P. Berzins, Peripheral NK1.1$^-$ NKT cells are mature and functionally distinct from their thymic counterparts. *J. Immunol.* **179**, 6630-6637 (2007).

20. A. K. Savage, M. G. Constantinides, J. Han, D. Picard, E. Martin, B. F. Li, O. Lantz, A. Bendelac, The transcription factor PLZF directs the effector program of the NKT cell lineage. *Immunity* **29**, 391-403 (2008).

21. W. Rabacal, S. K. Pabbisetty, K. L. Hoek, D. Cendron, Y. Guo, D. Maseda, E. Sebzda, Transcription factor KLF2 regulates homeostatic NK cell proliferation and survival. *Proc. Natl. Acad. Sci. U.S.A.* **113**, 5370-5375 (2016).

22. H. S. Tao, L. Li, N. S. Liao, K. S. Schluns, S. Luckhart, J. W. Sleasman, X. P. Zhong, Thymic epithelial cell-derived IL-15 and IL-15 receptor α chain foster local environment for type 1 innate like T cell development. *Front. Immunol.* **12**, 623280 (2021).

23. M. S. Anderson, E. S. Venanzi, L. Klein, Z. Chen, S. P. Berzins, S. J. Turley, H. von Boehmer, R. Bronson, A. Dierich, C. Benoist, D. Mathis, Projection of an immunological self shadow within the thymus by the aire protein. *Science* **298**, 1395-1401 (2002).

24. D. Levi, C. Polychronakos, Self-antigen expression in thymic epithelial cells in Ifn-γ or Tnf-α deficiency. *Cytokine* **62**, 433-438 (2013).

25. T. Olszak, D. D. An, S. Zeissig, M. P. Vera, J. Richter, A. Franke, J. N. Glickman, R. Siebert, R. M. Baron, D. L. Kasper, R. S. Blumberg, Microbial exposure during early life has persistent effects on natural killer T cell function. *Science* **336**, 489-493 (2012).

26. S. Y. Thomas, S. T. Scanlon, K. G. Griewank, M. G. Constantinides, A. K. Savage, K. A. Barr, F. Y. Meng, A. D. Luster, A. Bendelac, PLZF induces an intravascular surveillance program mediated by long-lived LFA-1-ICAM-1 interactions. *J. Exp. Med.* **208**, 1179-1188 (2011).

27. Q. Y. Liu, C. H. Kim, Control of tissue-resident invariant NKT cells by vitamin A metabolites and P2X7-mediated cell death. *J. Immunol.* **203**, 1189-1197 (2019).

28. E. Germanov, L. Veinotte, R. Cullen, E. Chamberlain, E. C. Butcher, B. Johnston, Critical role for the chemokine receptor CXCR6 in homeostasis and activation of CD1d-restricted NKT cells. *J. Immunol.* **181**, 81-91 (2008).

29. C. N. Skon, J. Y. Lee, K. G. Anderson, D. Masopust, K. A. Hogquist, S. C. Jameson, Transcriptional downregulation of S1pr1 is required for the establishment of resident memory $CD8^+$ T cells. *Nat. Immunol.* **14**, 1285-1293 (2013).

30. J. J. O'Konek, P. Illarionov, D. S. Khursigara, E. Ambrosino, L. Lzhak, B. F. Castillo, R. Raju, M. Khalili, H. Y. Kim, A. R. Howel, G. S. Besra, S. A. Porcelli, J. A. Berzofsky, M. Terabe, Mouse and human iNKT cell agonist β-mannosylceramide reveals a distinct mechanism of tumor immunity. *J. Clin. Invest.* **121**, 683-694 (2011).

31. R. M. McEwen-Smith, M. Salio, V. Cerundolo, The regulatory role of invariant NKT cells in tumor immunity. *Cancer Immunol. Res.* **3**, 425-435 (2015).

32. M. Bedard, M. Salio, V. Cerundolo, Harnessing the power of invariant natural killer T cells in cancer immunotherapy. *Front. Immunol.* **8**, 1829 (2017).

33. J. Schmieg, G. Yang, R. W. Franck, M. Tsuji, Superior protection against malaria and melanoma metastases by a C-glycoside analogue of the natural killer T cell ligand α-Galactosylceramide. *J. Exp. Med.* **198**, 1631-1641 (2003).

34. C. De Santo, M. Salio, S. H. Masri, L. Y. H. Lee, T. Dong, A. O. Speak, S. Porubsky, S. Booth, N. Veerapen, G. S. Besra, H. J. Groene, F. M. Platt, M. Zambon, V. Cerundolo, Invariant NKT cells reduce the immunosuppressive activity of influenza A virus-induced myeloid-derived suppressor cells in mice and humans. *J. Clin. Invest.* **118**, 4036-4048 (2008).

35. P. T. Lee, K. Benlagha, L. Teyton, A. Bendelac, Distinct functional lineages of human Vα24 natural killer T cells. *J. Exp. Med.* **195**, 637-641 (2002).

36. F. Ahmad, E. M. Shankar, Y. K. Yong, H. Y. Tan, G. Ahrenstorf, R. Jacobs, M. Larsson, R. E. Schmidt, A. Kamarulzaman, A. W. Ansari, Negative checkpoint regulatory molecule 2B4 (CD244) upregulation ss associated with invariant natural killer T cell alterations and human immunodeficiency virus disease progression. *Front. Immunol.* **8**, 338 (2017).

37. Y. Takahama, I. Ohigashi, S. Baik, G. Anderson, Generation of diversity in thymic epithelial cells. *Nat. Rev. Immunol.* **17**, 295-305 (2017).

38. B. Lucas, A. J. White, E. J. Cosway, S. M. Parnell, K. D. James, N. D. Jones, I. Ohigashi, Y. Takahama, W. E. Jenkinson, G. Anderson, Diversity in medullary thymic epithelial cells controls the activity and availability of iNKT cells. *Nat. Commun.* **11**, 2198 (2020).

39. E. C. Reilly, K. L. Emo, P. M. Buckley, N. S. Reilly, I. Smith, F. A. Chaves, H. M. Yang, P. W. Oakes, D. J. Topham, T_{RM} integrins CD103 and CD49a differentially support adherence and motility after resolution of influenza virus infection. *Proc. Natl. Acad. Sci. U.S.A.* **117**, 12306-12314 (2020).

40. P. Eissmann, L. Beauchamp, J. Wooters, J. C. Tilton, E. O. Long, C. Watzl, Molecular basis for positive and negative signaling by the natural killer cell receptor 2B4 (CD244).

Blood **105**, 4722-4729 (2005).

41. D. D. An, S. F. Oh, T. Olszak, J. F. Neves, F. Y. Avci, D. Erturk-Hasdemir, X. Lu, S. Zeissig, R. S. Blumberg, D. L. Kasper, Sphingolipids from a symbiotic microbe regulate homeostasis of host intestinal natural killer T cells. *Cell* **156**, 123-133 (2014).

42. S. Jasemi, M. Emaneini, Z. Ahmadinejad, M. S. Fazeli, L. A. Sechi, F. Sadeghpour Heravi, M. M. Feizabadi, Antibiotic resistance pattern of bacteroides fragilis isolated from clinical and colorectal specimens. *Ann. Clin. Microbiol. Antimicrob.* **20**, 27 (2021).

43. E. Tupin, Y. Kinjo, M. Kronenberg, The unique role of natural killer T cells in the response to microorganisms. *Nat. Rev. Microbiol.* **5**, 405-417 (2007).

44. N. Schmitz, M. Kurrer, M. F. Bachmann, M. Kopf, Interleukin-1 is responsible for acute lung immunopathology but increases survival of respiratory influenza virus infection. *J. Virol.* **79**, 6441-6448 (2005).

45. J. R. Teijaro, K. B. Walsh, S. Cahalan, D. M. Fremgen, E. Roberts, F. Scott, E. Martinborough, R. Peach, M. B. A. Oldstone, H. Rosen, Endothelial cells are central orchestrators of cytokine amplification during influenza virus infection. *Cell* **146**, 980-991 (2011).

46. M. F. Tavazoie, I. Pollack, R. Tanqueco, B. N. Ostendorf, B. S. Reis, F. C. Gonsalves, I. Kurth, C. Andreu-Agullo, M. L. Derbyshire, J. Posada, S. Takeda, K. N. Tafreshian, E. Rowinsky, M. Szarek, R. J. Waltzman, E. A. Mcmillan, C. N. Zhao, M. Mita, A. Mita, B. Chmielowski, M. A. Postow, A. Ribas, D. Mucida, S. F. Tavazoie, LXR/ApoE activation restricts innate immune suppression in cancer. *Cell* **172**, 825-840 (2018).

47. T. Ichinohe, I. K. Pang, Y. Kumamoto, D. R. Peaper, J. H. Ho, T. S. Murray, A. Iwasaki, Microbiota regulates immune defense against respiratory tract influenza A virus infection.

Proc. Natl. Acad. Sci. U.S.A. **108**, 5354-5359 (2011).

48. R. Nakamura, N. Maeda, K. Shibata, H. Yamada, T. Kase, Y. Yoshikai, Interleukin-15 is critical in the pathogenesis of influenza A virus-induced acute lung injury. *J. Virol.* **84**, 5574-5582 (2010).

49. J. E. Gumperz, S. Miyake, T. Yamamura, M. B. Brenner, Functionally distinct subsets of CD1d-restricted natural killer T cells revealed by CD1d tetramer staining. *J. Exp. Med.* **195**, 625-636 (2002).

50. Y. F. Yang, M. Tomura, M. Iwasaki, T. Mukai, P. Gao, S. Ono, J. P. Zou, G. M. Shearer, H. Fujiwara, T. Hamaoka, IL-12 as well as IL-2 upregulates CCR5 expression on T cell receptor-triggered human $CD4^+$ and $CD8^+$ T cells. *J. Clin. Immunol.* **21**, 116-125 (2001).

51. K. Miyauchi, A. Sugimoto-Ishige, Y. Harada, Y. Adachi, Y. Usami, T. Kaji, K. Inoue, H. Hasegawa, T. Watanabe, A. Hijikata, S. Fukuyama, T. Maemura, M. Okada-Hatakeyama, O. Ohara, Y. Kawaoka, Y. Takahashi, T. Takemori, M. Kubo, Protective neutralizing influenza antibody response in the absence of T follicular helper cells. *Nat. Immunol.* **17**, 1447-1458 (2016).

52. S. Zuklys, J. Gill, M. P. Keller, M. Hauri-Hohl, S. Zhanybekova, G. Balciunaite, K. J. Na, L. T. Jeker, K. Hafen, N. Tsukamoto, T. Amagai, M. M. Taketo, W. Krenger, G. A. Hollander, Stabilized β-catenin in thymic epithelial cells blocks thymus development and function. *J. Immunol.* **182**, 2997-3007 (2009).

53. Y. Y. Kisanuki, R. E. Hammer, J. Miyazaki, S. C. Williams, J. A. Richardson, M. Yanagisawa, Tie2-Cre transgenic mice: a new model for endothelial cell-lineage analysis in vivo. *Dev. Biol.* **230**, 230-242 (2001).

54. P. P. Lee, D. R. Fitzpatrick, C. Beard, H. K. Jessup, S. Lehar, K. W. Makar, M. Perez-

Melgosa, M. T. Sweetser, M. S. Schlissel, S. Nguyen, S. R. Cherry, J. H. Tsai, S. M. Tucker, W. M. Weaver, A. Kelso, R. Jaenisch, C. B. Wilson, A critical role for Dnmt1 and DNA methylation in T cell development, function, and survival. *Immunity* **15**, 763-774 (2001).

55. M. L. Caton, M. R. Smith-Raska, B. Reizis, Notch-RBP-J signaling controls the homeostasis of $CD8^-$ dendritic cells in the spleen. *J. Exp. Med.* **204**, 1653-1664 (2007).

56. B. E. Clausen, C. Burkhardt, W. Reith, R. Renkawitz, I. Forster, Conditional gene targeting in macrophages and granulocytes using LysMcre mice. *Transgenic Res.* **8**, 265-277 (1999).

57. D. Unutmaz, W. K. Xiang, M. J. Sunshine, J. Campbell, E. Butcher, D. R. Littman, The primate lentiviral receptor Bonzo/STRL33 is coordinately regulated with CCR5 and its expression pattern is conserved between human and mouse. *J. Immunol.* **165**, 3284-3292 (2000).

58. S. T. Smiley, M. H. Kaplan, M. J. Grusby, Immunoglobulin E production in the absence of interleukin-4-secreting CD1-dependent cells. *Science* **275**, 977-979 (1997).

59. S. Itohara, P. Mombaerts, J. Lafaille, J. Iacomini, A. Nelson, A. R. Clarke, M. L. Hooper, A. Farr, S. Tonegawa, T cell receptor delta gene mutant mice: independent generation of αβ T cells and programmed rearrangements of γδ TCR genes. *Cell* **72**, 337-348 (1993).

60. T. Hato, Y. Kimura, T. Morisada, G. Y. Koh, K. Miyata, M. Tabata, T. Kadomatsu, M. Endo, T. Urano, F. Arai, K. Araki, T. Suda, K. Kobayashi, Y. Oike, Angiopoietins contribute to lung development by regulating pulmonary vascular network formation. *Biochem. Biophys. Res. Commun.* **381**, 218-223 (2009).

61. G. W. Cui, A. Shimba, G. Y. Ma, K. Takahara, S. Tani-ichi, Y. B. Zhu, T. Asahi, A. Abe,

H. Miyachi, S. Kitano, T. Hara, J. Yasunaga, H. Suwanai, H. Yamada, M. Matsuoka, K. Ueki, Y. Yoshikai, K. Ikuta, IL-7R-dependent phosphatidylinositol 3-kinase competes with the STAT5 signal to modulate T cell development and homeostasis. *J. Immunol.* **204**, 844-857 (2020).

62. Y. B. Zhu, G. W. Cui, E. Miyauchi, Y. Nakanishi, H. Mukohira, A. Shimba, S. Abe, S. Tani-Ichi, T. Hara, H. Nakase, T. Chiba, A. Sehara-Fujisawa, H. Seno, H. Ohno, K. Ikuta, Intestinal epithelial cell-derived IL-15 determines local maintenance and maturation of intra-epithelial lymphocytes in the intestine. *Int. Immunol.* **32**, 307-319 (2020).

63. H. G. Wang, E. R. Breed, Y. J. Lee, L. J. Qian, S. C. Jameson, K. A. Hogquist, Myeloid cells activate iNKT cells to produce IL-4 in the thymic medulla. *Proc. Natl. Acad. Sci. U.S.A.* **116**, 22262-22268 (2019).

64. K. Shiroguchi, T. Z. Jia, P. A. Sims, X. S. Xie, Digital RNA sequencing minimizes sequence-dependent bias and amplification noise with optimized single-molecule barcodes. *Proc. Natl. Acad. Sci. U.S.A.* **109**, 1347-1352 (2012).

65. T. Ogawa, K. Kryukov, T. Imanishi, K. Shiroguchi, The efficacy and further functional advantages of random-base molecular barcodes for absolute and digital quantification of nucleic acid molecules. *Sci. Rep.* **7**, 13576 (2017).

66. M. Tenno, K. Shiroguchi, S. Muroi, E. Kawakami, K. Koseki, K. Kryukov, T. Imanishi, F. Ginhoux, I. Taniuchi, Cbfβ 2 deficiency preserves Langerhans cell precursors by lack of selective TGF beta receptor signaling. *J. Exp. Med.* **214**, 2933-2946 (2017).

67. M. I. Love, W. Huber, S. Anders, Moderated estimation of fold change and dispersion for RNA-seq data with DESeq2. *Genome Biol.* **15**, (2014).

68. Y. Y. Zhou, B. Zhou, L. Pache, M. Chang, A. H. Khodabakhshi, O. Tanaseichuk, C.

Benner, S. K. Chanda, Metascape provides a biologist-oriented resource for the analysis of systems-level datasets. *Nat. Commun.* **10**, 1523 (2019).

69. G. Gasteiger, X. Y. Fan, S. Dikiy, S. Y. Lee, A. Y. Rudensky, Tissue residency of innate lymphoid cells in lymphoid and nonlymphoid organs. *Science* **350**, 981-985 (2015).

70. S. Haddadi, N. Thanthrige-Don, S. Afkhami, A. Khera, M. Jeyanathan, Z. Xing, Expression and role of VLA-1 in resident memory CD8 T cell responses to respiratory mucosal viral-vectored immunization against tuberculosis. *Sci. Rep.* **7**, 9525 (2017).

71. N. Y. Crowe, J. M. Coquet, S. P. Berzins, K. Kyparissoudis, R. Keating, D. G. Pellicci, Y. Hayakawa, D. I. Godfrey, M. J. Smyth, Differential antitumor immunity mediated by NKT cell subsets in vivo. *J. Exp. Med.* **202**, 1279-1288 (2005).

72. T. Kawano, J. Cui, Y. Koezuka, I. Toura, Y. Kaneko, H. Sato, E. Kondo, M. Harada, H. Koseki, T. Nakayama, Y. Tanaka, M. Taniguchi, Natural killer-like nonspecific tumor cell lysis mediated by specific ligand-activated Vα14 NKT cells. *Proc. Natl. Acad. Sci. U.S.A.* **95**, 5690-5693 (1998).

73. K. G. Anderson, K. Mayer-Barber, H. Sung, L. Beura, B. R. James, J. J. Taylor, L. Qunaj, T. S. Griffith, V. Vezys, D. L. Barber, D. Masopust, Intravascular staining for discrimination of vascular and tissue leukocytes. *Nat. Protoc.* **9**, 209-222 (2014).

74. S. M. Caucheteux, P. Torabi-Parizi, W. E. Paul, Analysis of naive lung CD4 T cells provides evidence of functional lung to lymph node migration. *Proc. Natl. Acad. Sci. U.S.A.* **110**, 1821-1826 (2013).

FIGURE captions

Fig. 1. Characterization of mouse C2 iNKT cells.

(A) Gating strategy for C2 iNKT ($CD244^{+}CXCR6^{+}$), C1 iNKT ($CD244^{-}CXCR6^{+}$), and C0 iNKT ($CD244^{-}CXCR6^{-}$) cells in mature iNKT cells in the thymus. **(B)** Flow cytometric analysis of the IFN-γ/Venus expression in thymic iNKT cell populations of IFN-γ-Venus reporter mice at steady state. **(C)** *IFN-γ* mRNA levels relative to *Hprt* in C2 and C1 iNKT cells were measured by qPCR (n = 3). **(D)** Flow cytometric analysis of PLZF expression in the indicated thymic iNKT cell subsets. **(E)** Flow cytometric analysis of NKT1, NKT2, and NKT17 populations in thymic C2 and C1 iNKT cells in mice. **(F)** Flow cytometric analysis of CD4 expression in thymic C2 and C1 iNKT cells. **(G)** Principal component analysis (PCA) performed on thymic C2, C1, and C0 iNKT cells. Expression data were measured by dRNA-seq. **(H)** Heat map of selected genes that were differentially expressed between thymic C2 and C1 iNKT cells ($p \leq 0.01$) from three biological replicates. **(I)** Bar chart depicting the functional analysis of differentially expressed genes between thymic C2 and C1 iNKT cells. Normalized enrichment scores were calculated using Metascape. **(J)** The mRNA expression levels of transcription factor *Klf2* relative to *Hprt* in C2 and C1 iNKT cells measured by qPCR (n = 3). **(K)** Flow cytometric analysis of ICOS expression in C2 and C1 iNKT cells. **(L)** PCA performed on C2, C1, and C0 iNKT cells, and CD4 SP, CD8 SP, and NK cells. Expression data were measured by dRNA-seq. **(M)** Frequency of C2, C1, and C0 iNKT cells in the mature $NK1.1^{+}$ iNKT population in the thymus of 1- to 48-week-old (wks) specific pathogen-free (SPF) mice (n = 4 per each time point). **(N)** Frequency of C2 iNKT cells in the mature $NK1.1^{+}$ iNKT population of the indicated peripheral tissues (n = 5 per each tissue). BM, bone marrow; Adipo, adipose tissue; LP, lamina propria; PBL, peripheral

blood lymphocytes. Data represent at least three independent experiments with similar results (A, B, D, E, F, and K). Data are means ± SEM and pooled from three separate mice with duplicate measurement per mouse (C and J); Student's *t*-test. Data are means ± SD and pooled from 3-4 independent experiments (M and N). **, $p < 0.01$.

Fig. 2. The thymic IL-15 niche is essential for the development and maturation of C2 iNKT cells.

(A) Number of iNKT cells at stages 1, 2, and 3 in the thymus of FoxN1-Cre IL-15 cKO mice (FoxN1; IL-15 cKO) and littermate control mice (Control) (n = 5). **(B)** Number of NKT1, NKT2, and NKT17 cells in the thymus of FoxN1-Cre IL-15 cKO mice and littermate control mice (n = 4). **(C)** Flow cytometric analysis for anti-apoptotic factor Bcl-2 and Bcl-xL expression in mature NK1.1$^+$ iNKT cells in FoxN1-Cre IL-15 cKO mice and littermate control mice. **(D)** Frequency of Ki-67$^+$ cells in mature iNKT cells of FoxN1-Cre IL-15 cKO mice and littermate control mice (n = 4). **(E and F)** Flow cytometric analysis (E) and number (F) of C2, C1, and C0 iNKT cells in the thymus of FoxN1-Cre IL-15 cKO mice or littermate control mice (n = 10). **(G)** Number of NK cells (n = 4) and MAIT cells (n = 5) in the thymus of FoxN1-Cre IL-15 cKO mice and littermate control mice. **(H and I)** Flow cytometric analysis (H) and frequency (I) of iNKT cells 4 days after the culture of freshly isolated thymic C2, C1, and C0 iNKT cells with (+) or without (−) IL-15 (n = 4). **(J)** Wild-type mice were administered IL-15/IL-15Rα complex (RLI) or control PBS (Control) by intravenous injection every two days. Frequency of thymic C2, C1, and C0 iNKT cells in whole iNKT cells 4 days after the first administration (n = 4). **(K)** CD45.1 C0 iNKT cells were injected into the thymus of CD45.2 wild-type mice, and the frequency of C2 and C1 iNKT cells in CD45.1 iNKT cells was assessed 4 days later (n = 4). **(L)** FoxN1-Cre IL-15 cKO (cKO) mice or littermate control mice (Con) were administered α-galactosylceramide (α-Gal) (+) or control PBS (−) by intraperitoneal injection every two days. The frequency of thymic C2, C1, and C0 iNKT cells in thymocytes 4 days after the first administration (n = 4). Data are mean ± SD and pooled from 3-5 independent experiments; Student's *t*-test or *t*-test with Welch's correction (A, B, D, F, G and J) and one-way or two-way ANOVA (I and L). Data

represent at least three independent experiments with similar results (C, E, H and K). **, $p < 0.01$; *, $p < 0.05$; n.s., not significant.

Fig. 3. Developmental and functional regulation of C2 iNKT cells in the thymus.

(A) Number of thymic C2, C1, and C0 iNKT cells in FoxN1-Cre IL-15Rα cKO mice (FoxN1; IL-15Rα cKO) and littermate control mice (Control) (n = 5). **(B)** Lethally irradiated hosts (Tie2-Cre IL-15 cKO mice or littermate control mice, CD45.2) were reconstituted with bone marrow cells in wild-type mice (CD45.1). Number of donor-derived thymic C2, C1, and C0 iNKT cells in hosts after bone marrow transplantation (BMT) (n = 5). **(C and D)** Number of thymic C2 and C1 iNKT cells in LysM-Cre IL-15 cKO mice (LysM; IL-15 cKO) (n = 4) (C) and CD11c-Cre IL-15 cKO mice (CD11c; IL-15 cKO) (n = 5) (D) with littermate control mice (Control). **(E)** Immunohistochemistry of iNKT cells in the thymus of IL-15-CFP knock-in (KI) mice. White arrows indicate iNKT cells (PBS57-loaded CD1d-tetramer^{+}TCRβ^{+}). Boxed areas in the upper panels are enlarged in the lower panels (n = 3). M, thymic medulla. Scale bars, 50 μm. **(F)** Frequency of CD4 SP, CD8 SP, and iNKT cells in contact with IL-15-expressing cells in the thymic medulla detected by immunohistochemistry as shown in (E) and fig. S5B (n = 3). **(G and H)** Flow cytometric analysis of IFN-γ/Venus expression in the indicated thymocytes of IFN-γ-Venus reporter mice. **(I)** *Aire* and *Ins2* mRNA levels relative to *Hprt* in freshly isolated medullary thymic epithelia cells (mTECs) in FoxN1-Cre IL-15 cKO mice (FoxN1; IL-15 cKO) or littermate control mice (Control) measured by qPCR (n = 3). **(J)** Immunohistochemistry for Aire^{+} mTECs in FoxN1-Cre IL-15 cKO mice and littermate control mice (n = 3). Scale bars, 50 μm. **(K)** *Aire* mRNA levels relative to *Hprt* in freshly isolated medullary thymic epithelia cells (mTECs) from FoxN1-Cre IL-15 cKO × CD1d1/2 KO mice (FoxN1; IL-15 cKO; CD1d1/2 KO) or littermate control CD1d1/2 KO mice were measured by qPCR (n = 3). Data are means ± SD and pooled from 4-5 independent experiments (A, B, C, and D); Student's *t*-test or *t*-test with Welch's correction. Data represent at least three independent experiments with similar results (G

and H). Data represent three separate mice with similar results (E and J). Data are means ± SEM and pooled from three separate mice with duplicate measurements per mouse; one-way ANOVA (F) and Student's *t*-test (I and K). **, $p < 0.01$; *, $p < 0.05$; n.s., not significant.

Fig. 4. Characterization of peripheral C2 and C1 iNKT cells.

(A and B) Flow cytometric analysis (A) and number (B) of C2 and C1 iNKT cells in the lung of FoxN1-Cre IL-15 cKO mice (FoxN1; IL-15 cKO) or littermate control mice (Control) (n = 8). **(C and D)** Number of C2 and C1 iNKT cells in the spleen (C) (n = 6) and peripheral blood lymphocytes (PBL) (D) in FoxN1-Cre IL-15 cKO mice and littermate control mice (n = 4). **(E)** PCA between lung C2 and C1 iNKT cells. Expression data were measured by dRNA-seq. **(F)** Heat map of selected genes that were differentially expressed between lung C2 and C1 iNKT cells ($p \leq 0.01$) from three biological replicates. Gene names shown in blue displayed similar expression patterns with those in the thymus. **(G)** Intravascular staining with anti-CD45 antibody administered intravenously 3 min before the isolation of the indicated lymphocyte populations. Frequency of $CD45^+$ intravascular cells in each population is shown. **(H)** Frequency of $CD45^+$ intravascular cells among the indicated lymphocytes by intravascular staining of CD45, as shown in (G) (n = 4). **(I and J)** Number of lung C2 and C1 iNKT cells and NK cells in LysM-Cre IL-15 cKO mice (LysM; IL-15 cKO) (I) and SPC-Cre IL-15 cKO mice (SPC; IL-15 cKO) (J) with littermate control mice (n = 5). Data represent at least three independent experiments with similar results (A and G). Data are means ± SD and pooled from 3-5 independent experiments; Student's *t*-test or *t*-test with Welch's correction (B, C, D, I, and J) and one-way ANOVA (H). **, $p < 0.01$; *, $p < 0.05$; n.s., not significant.

Fig. 5. Distinct cell dynamics of C2 and C1 iNKT cells.

(A to D) Genetically marked CD45.1 and CD45.2 mice of the same age underwent parabiosis surgery and were analyzed after 60 days. Flow cytometric analysis for partner-derived and host-derived cells in peripheral C2 and C1 iNKT cells of the lung (A) and spleen (C). Frequency of partner-derived cells in C2 and C1 iNKT cells in the lung (B) (n = 9) and spleen (D) (n = 8). **(E and F)** Flow cytometric analysis (E) and mean fluorescence intensities (MFI) (F) of P2X7R expression between lung C2 and C1 iNKT cells (n = 3). **(G and H)** Flow cytometric analysis for partner-derived and host-derived cells in C2 and C1 iNKT cells of the bone marrow (BM) of parabionts (G). Frequency of partner-derived cells in BM C2 and C1 iNKT cells (H) (n = 5). **(I)** Flow cytometric analysis of partner-derived and host-derived cells in the indicated thymic iNKT cells 60 days after parabiosis surgery using same-aged CD45.1 and CD45.2 mice. **(J and K)** Flow cytometric analysis (J) and MFI (K) of P2X7R expression between thymic C2 and C1 iNKT cells (n = 3). **(L)** Number of lung C2 and C1 iNKT cells in CXCR6-GFP/GFP mice (CXCR6 KO) and wild-type (WT) mice (n = 4). **(M)** WT mice were administered anti-integrin α1 (α-CD49a) blocking antibody or isotype control (Iso) by intravenous injection every two days. Number of lung C2 and C1 iNKT cells 6 days after the first antibody administration (n = 4). Data represent at least two independent experiments with similar results (A, C, E, G, I, and J). Data are means ± SD (B, D, H, L, and M) or ± SEM (F and K); Student's *t*-test and pooled from 2-4 independent experiments. **, $p < 0.01$; *, $p < 0.05$; n.s., not significant.

Fig. 6. C2 iNKT cells enhance anti-tumor immunity.

(A and B) FoxN1-Cre IL-15 cKO mice (FoxN1; IL-15 cKO) or littermate control mice (Control) were administered 4×10^4 B16-F10 melanoma cells by intravenous injection. The lung metastasis (A) and number of metastatic nodules (B) in the lung after 14 days of inoculation with melanoma cells (n = 9). **(C)** FoxN1-Cre IL-15 cKO (cKO) mice or littermate control mice (Con) were administered 4×10^4 B16-F10 melanoma cells (+) or control PBS (−) 14 days before the analysis. Number of C2 and C1 iNKT cells and NK cells in the lung are shown. **(D)** Frequency of $KLRG1^+$ NK cells in the total NK population in the lungs of FoxN1-Cre IL-15 cKO mice and littermate control mice after 14 days of inoculation with B16-F10 melanoma cells (n = 5). **(E)** Frequency of $Ki\text{-}67^+$ cells in NK cells in FoxN1-Cre IL-15 cKO mice and littermate control mice after 14 days of inoculation with B16-F10 melanoma cells (n = 5). **(F)** The number of metastatic nodules in the lung of FoxN1-Cre IL-15 cKO × CD1d1/2 KO mice (FoxN1; IL-15 cKO; CD1d1/2 KO) or littermate control CD1d1/2 KO mice after 14 days of inoculation with B16-F10 melanoma cells (n = 5). **(G)** Flow cytometric analysis of IFN-γ expression in lung CD8 T cells, NK cells, and C2 and C1 iNKT cells in IFN-γ-Venus reporter mice after 14 days of inoculation with B16-F10 melanoma cells. **(H)** Flow cytometric analysis of granzyme B expression in lung C2 and C1 iNKT cells after 14 days of inoculation with B16-F10 melanoma cells. **(I and J)** Flow cytometric analysis for granzyme B (I) and perforin (J) expression in the indicated lung lymphocytes after 12 hours culture with B16-F10 melanoma cells in the presence of IL-15. **(K)** Target tumor cell viability in the tumor inhibition assay. Effector cells (C2 and C1 iNKT cells or NK cells) were isolated from B16-F10-inoculated and α-galactosylceramide-stimulated wild-type mice. The effector cells and B16-F10 tumor target cells were co-cultured at the indicated E:T ratios (n = 6). **(L and M)** CD45.1 C2 iNKT cells were adoptively transferred into CD45.2

FoxN1-Cre IL-15 cKO mice. Number of metastatic nodules (L) and C1 iNKT cells and NK cells (M) in recipients after 14 days of inoculation with B16-F10 melanoma cells (n = 5). **(N)** Frequency of $KLRG1^{+}$ NK cells in total NK cells in the lungs of FoxN1-Cre IL-15 cKO mice with or without the adoptive transfer of C2 iNKT cells after 14 days of inoculation with B16-F10 melanoma cells (n = 5). **(O)** Flow cytometric analysis of the IFN-γ expression in the indicated lung lymphocytes in CD45.2 FoxN1-Cre IL-15 cKO × IFN-γ-Venus reporter mice with or without the adoptive transfer of C2 iNKT cells after 14 days of inoculation with B16-F10 melanoma cells. Data represent at least three independent experiments with similar results (A, G, H, I, J, and O). Data are means ± SD and pooled from 2-5 independent experiments; Student's *t*-test (B, D, E, F, L, M, and N) or one-way ANOVA (C and K). **, $p < 0.01$; *, $p < 0.05$; n.s., not significant.

Fig. 7. C2 iNKT cells enhance anti-viral immune responses.

(A) FoxN1-Cre IL-15 cKO × IFN-γ-Venus reporter mice were intranasally administered with a 0.5 LD_{50} dose of IAV PR8. IFN-γ expression in lung CD8 T cells, NK cells, and C2 and C1 iNKT cells 7 days later. **(B)** Virus titers in the lung of FoxN1-Cre IL-15 cKO mice (FoxN1; IL-15 cKO) or littermate control mice (Control) after 4 days of infection with the 0.5 LD_{50} dose of IAV assessed by the $TCID_{50}$ assay (n = 5). **(C)** Number of C2 and C1 iNKT cells in the lung of FoxN1-Cre IL-15 cKO mice and control mice after 7 days of infection with the 0.5 LD_{50} dose of PR8 (n = 6). **(D and E)** Flow cytometric analysis (D) and frequency or number (E) of influenza $NP_{366-374}$-specific CD8 T cells in the lung of FoxN1-Cre IL-15 cKO or control mice on day 7 post infection (n = 6). **(F)** Number of NK cells, CD8 and CD4 T cells in the lung of FoxN1-Cre IL-15 cKO or control mice on day 7 post infection (n = 6). **(G)** Virus titers in the lung of FoxN1-Cre IL-15 cKO × CD1d1/2 KO mice (FoxN1; IL-15 cKO; CD1d1/2 KO) or control CD1d1/2 KO mice after 4 days of IAV infection assessed by the $TCID_{50}$ assay (n = 4). **(H)** Frequency and number of myeloid-derived suppressor cells (MDSCs) in the lung myeloid cells of FoxN1-Cre IL-15 cKO or control mice on day 7 post infection (n = 6). **(I to M)** CD45.1 C2 iNKT cells were adoptively transferred into CD45.2 FoxN1-Cre IL-15 cKO mice by intravenous injection. Virus titers in the lung of CD45.2 FoxN1-Cre IL-15 cKO recipients after 4 days of infection with the 0.5 LD_{50} dose of IAV assessed by $TCID_{50}$ assay (I) (n = 6). Number of C1 iNKT cells (J), influenza $NP_{366-374}$-specific CD8 T cells (K), CD8 T cells (K), NK cells (L), and MDSCs (M) in the lung after 7 days of infection (n = 5-6). **(N)** Flow cytometric analysis of IFN-γ expression in the indicated lung lymphocytes of FoxN1-Cre IL-15 cKO × IFN-γ-Venus reporter mice with or without the adoptive transfer of C2 iNKT cells after 7 days of infection with the 0.5 LD_{50} dose of IAV. Data represent at least three independent experiments with similar results (A, D, and N).

Data are means ± SD and pooled from 2-4 independent experiments; with Student's *t*-test (B, C, and E-M); Student's *t*-test. **, $p < 0.01$; *, $p < 0.05$; n.s., not significant.

Fig. 8. Characterization of human C2 iNKT cells.

(A) Flow cytometric analysis of human C2 ($CD244^{+}CXCR6^{+}$) and C1 ($CD244^{-}CXCR6^{+}$) iNKT cells in the peripheral blood of young and aged donors. **(B)** Flow cytometric analysis of CD4 expression in human C2 and C1 iNKT cells. **(C)** Frequency of human C2 iNKT cells in the peripheral blood of young donors (n = 5) and aged donors (n = 2), as shown in (A). **(D)** Frequency of IFN-γ^{+} cells in human C2 and C1 iNKT cells after stimulation with 25 ng/mL PMA and 1 μg/mL ionomycin for 4 hours (n = 4). **(E)** Principal component analysis (PCA) performed on human C2 and C1 iNKT cells. Expression data were measured by dRNA-seq. **(F)** Heat map of selected genes that were differentially expressed between human C2 and C1 iNKT cells ($p \leq 0.01$) from four biological replicates. **(G)** Bar chart depicting the functional analysis of differentially expressed genes between human C2 and C1 iNKT cells. Normalized enrichment scores were calculated using Metascape. **(H)** Flow cytometric analysis of CD161, CD94, CCR5, and ICOS expression in human C2 and C1 iNKT cells. Data represent at least two independent experiments with similar results (A, B, and H). Data are means ± SD and pooled from 2-3 independent experiments (C and D); with Student's *t*-test. *, $p < 0.05$.

Fig. 1

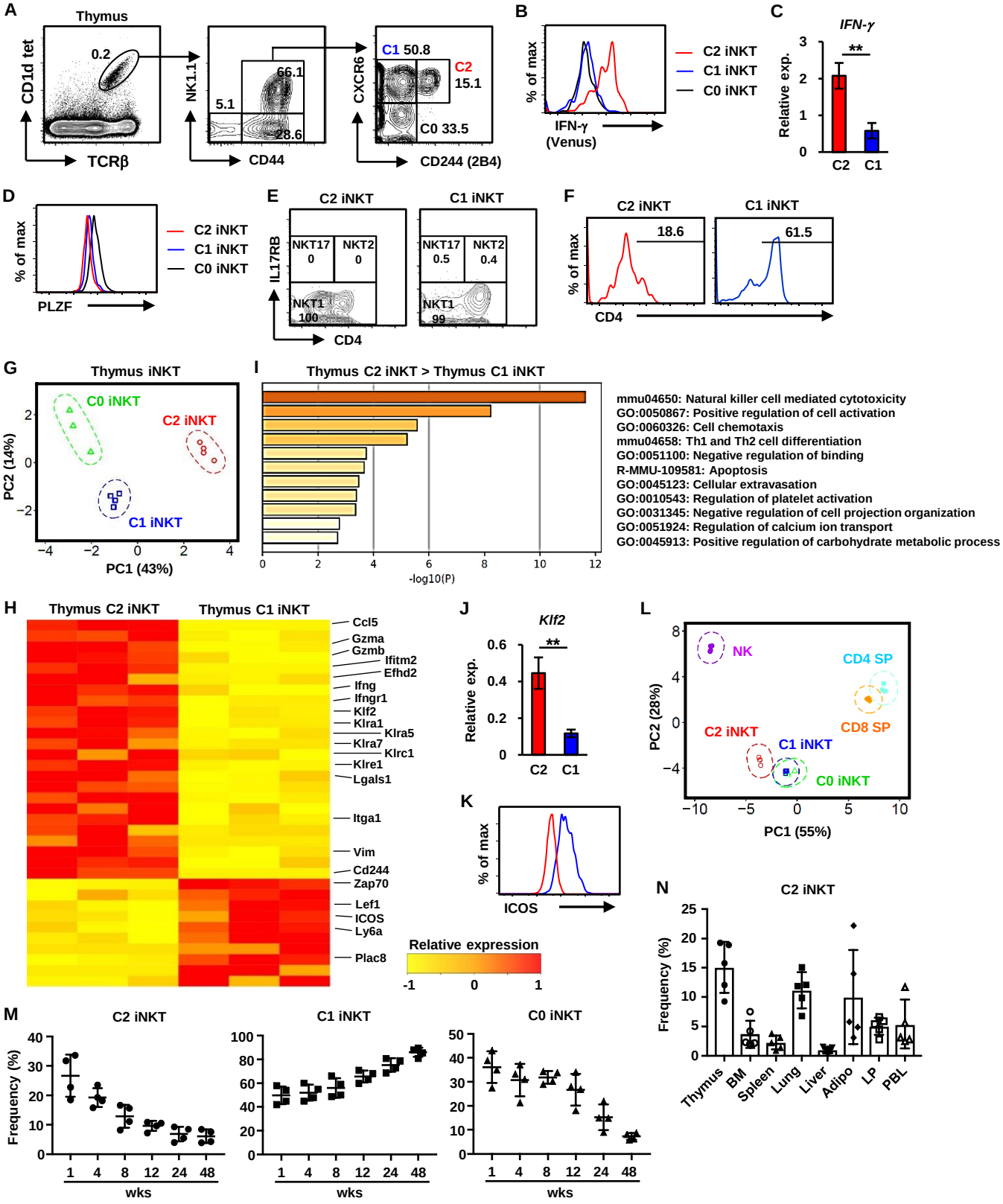

Fig. 2

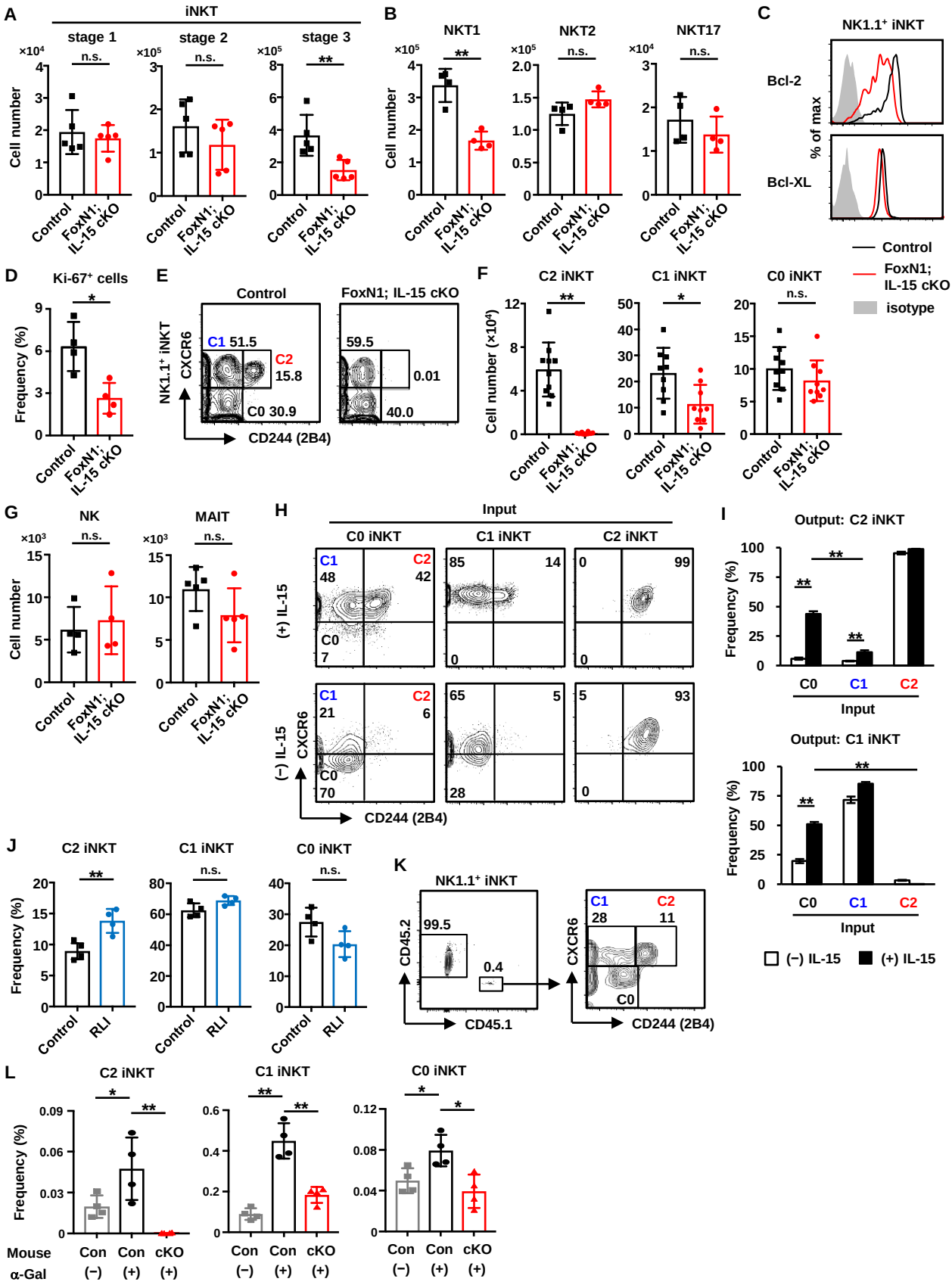

Fig. 3

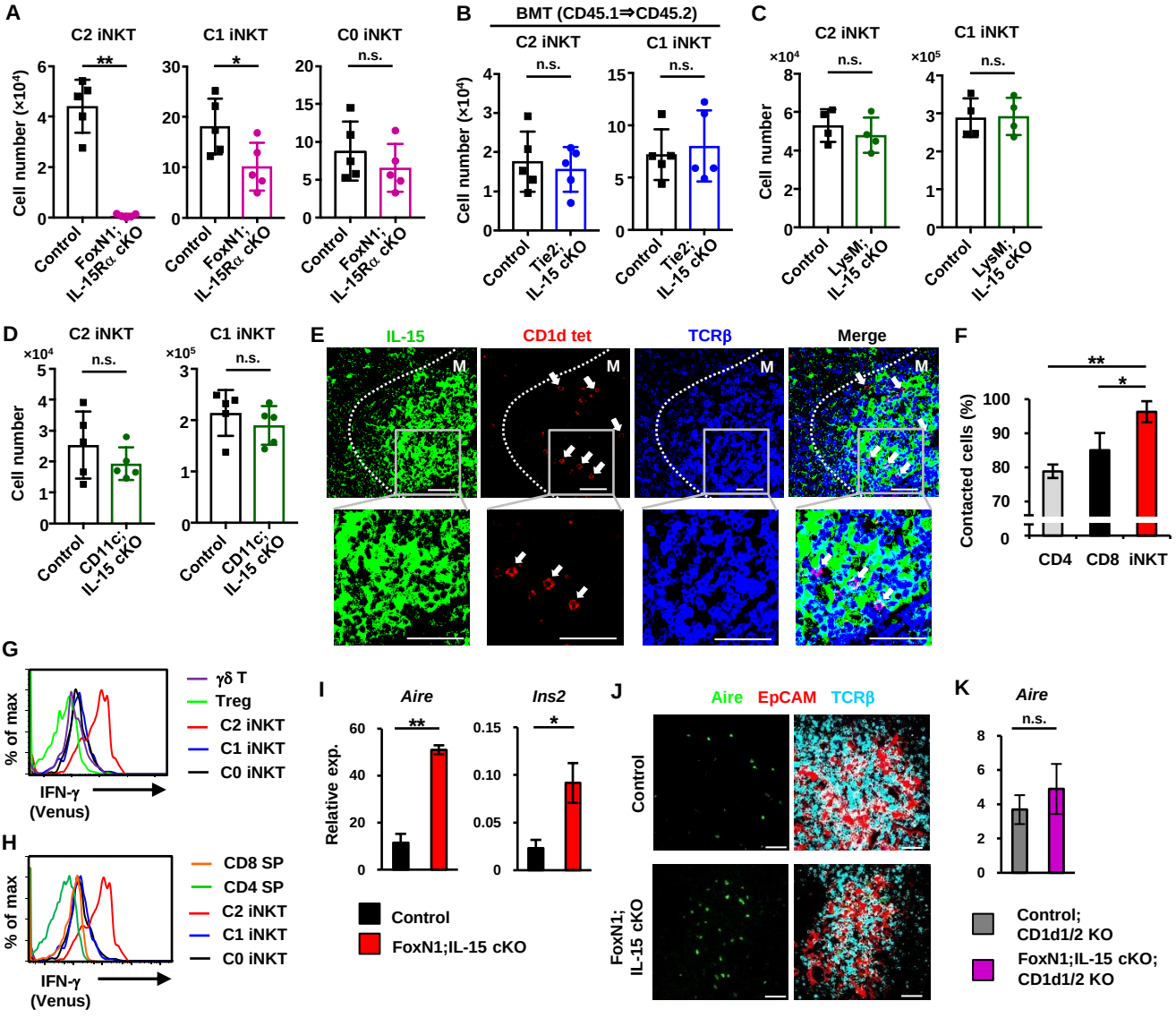

Fig. 4

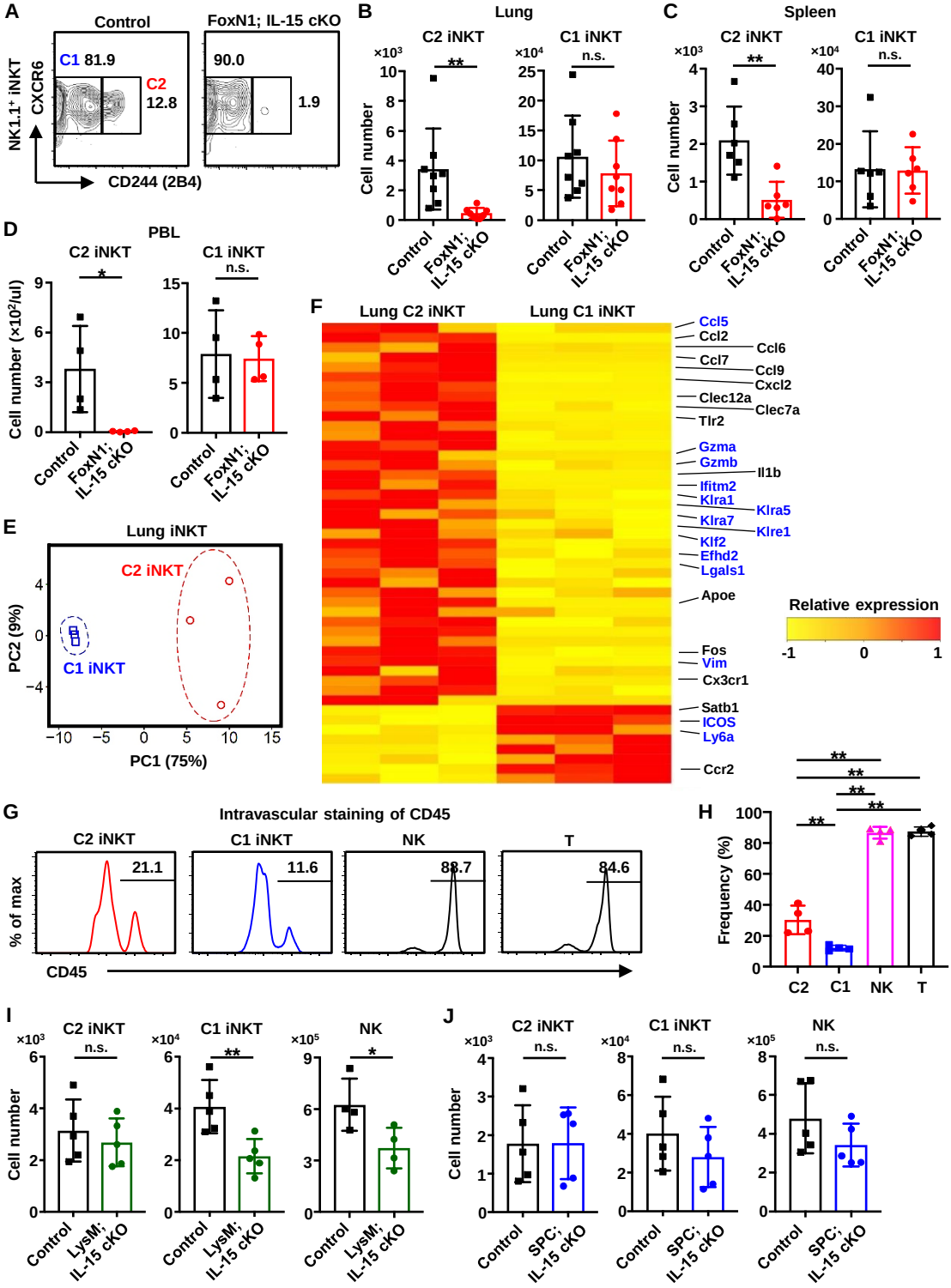

Fig. 5

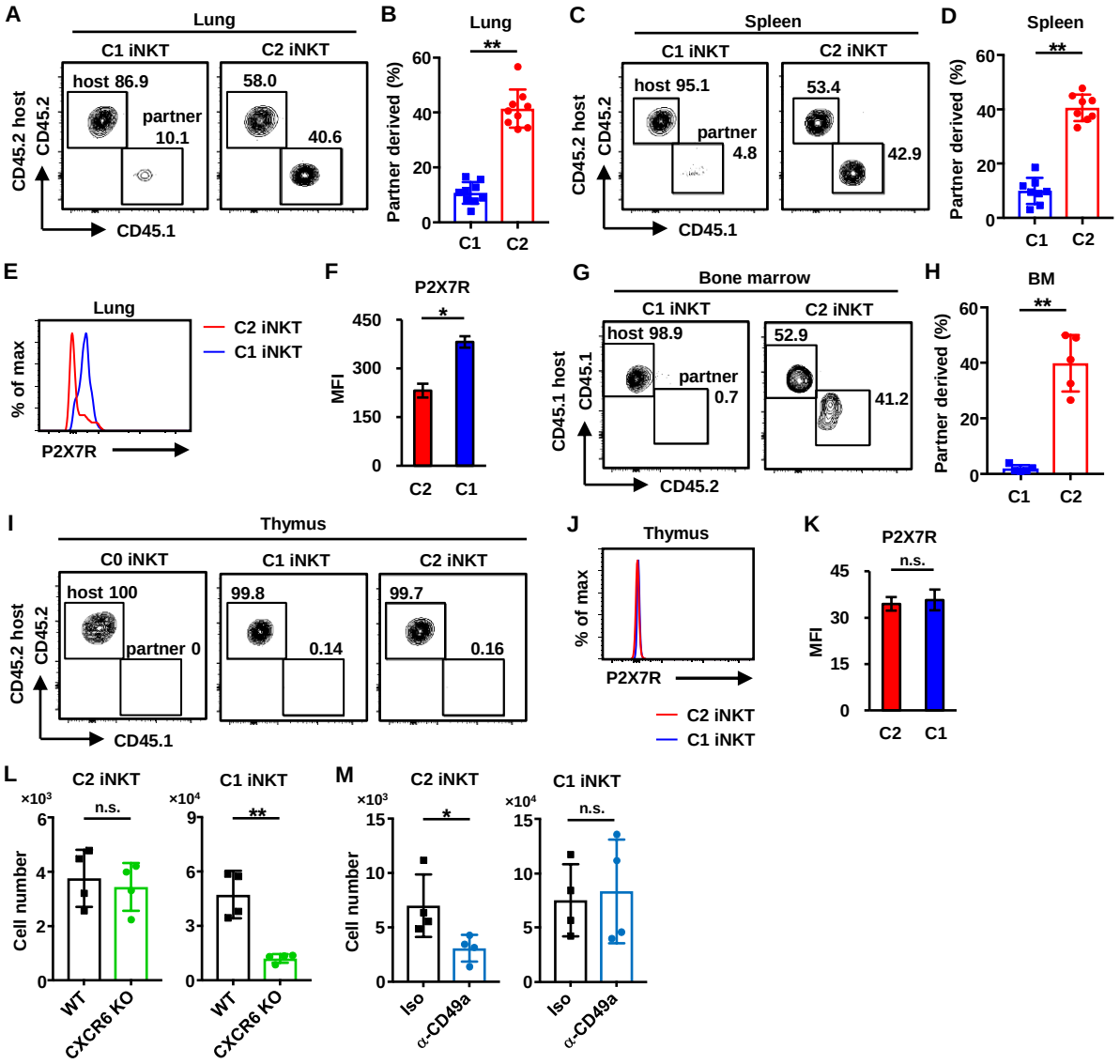

Fig. 6

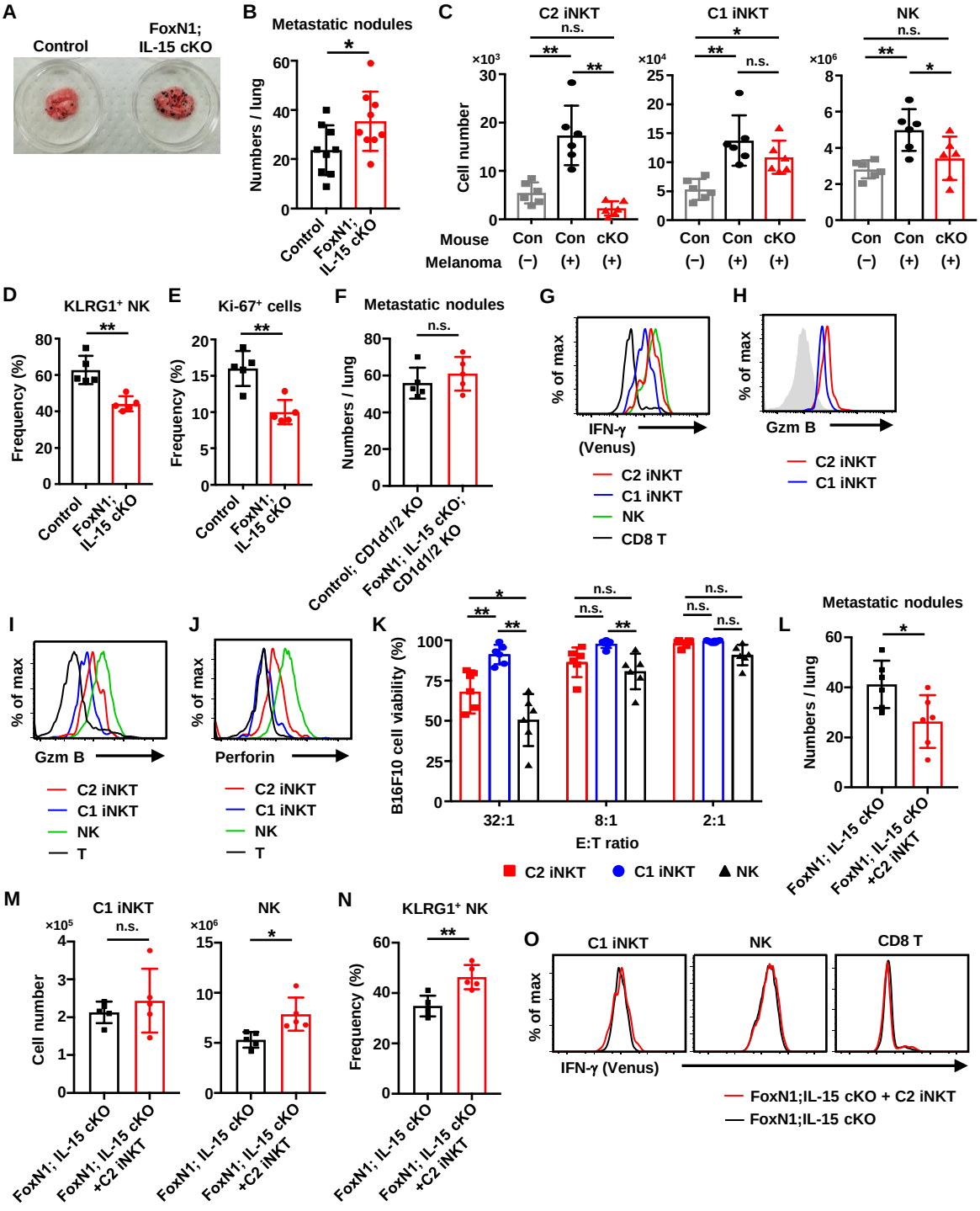

Fig. 7

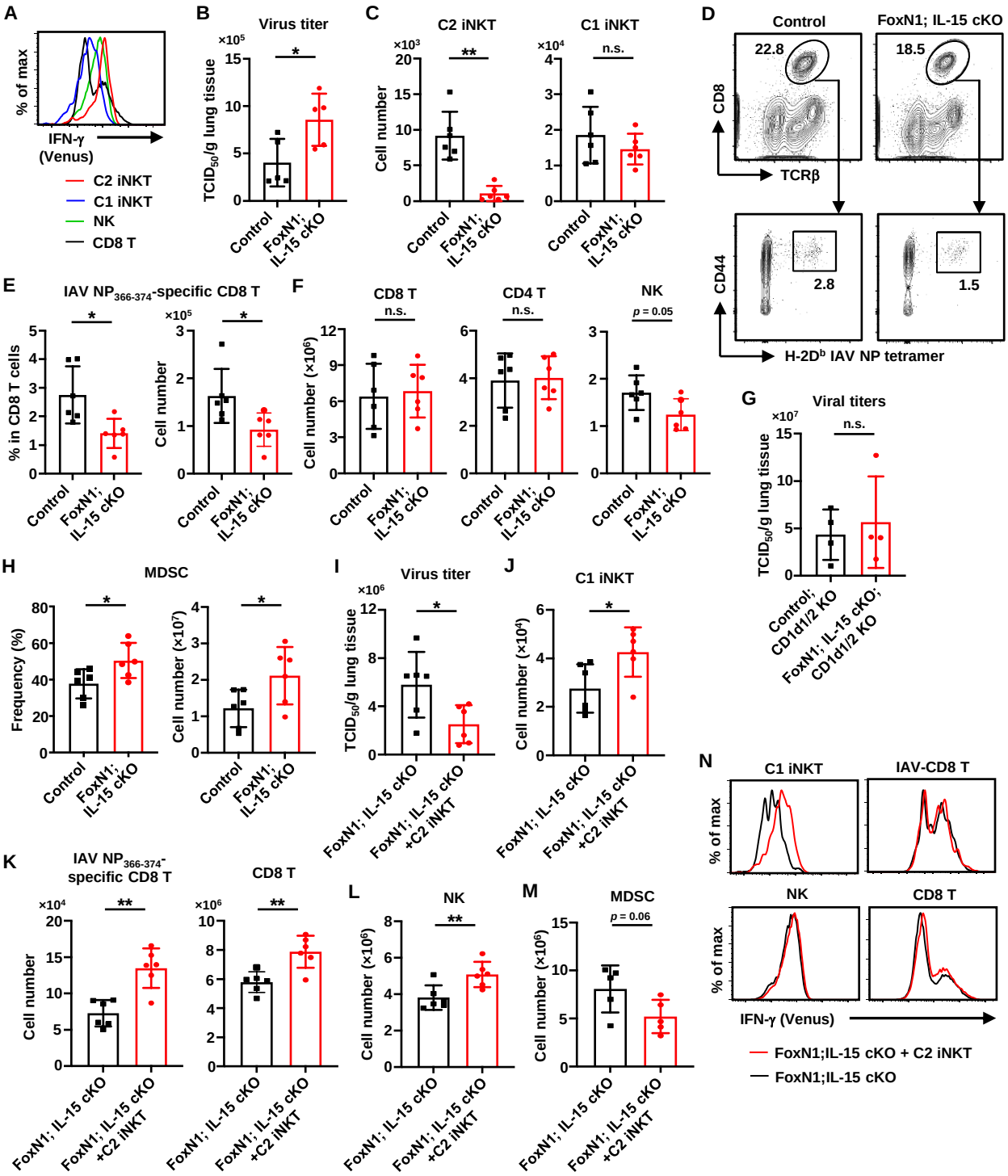

Fig. 8

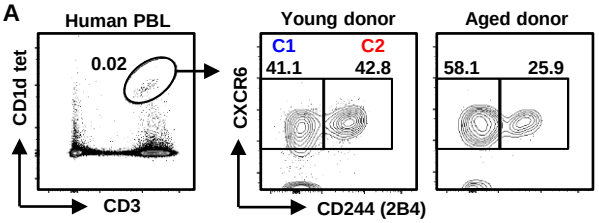

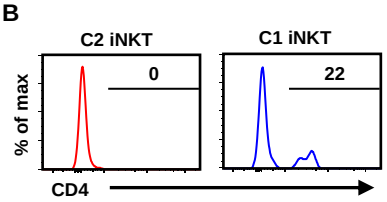

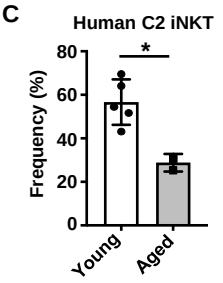

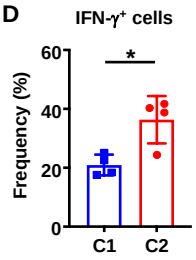

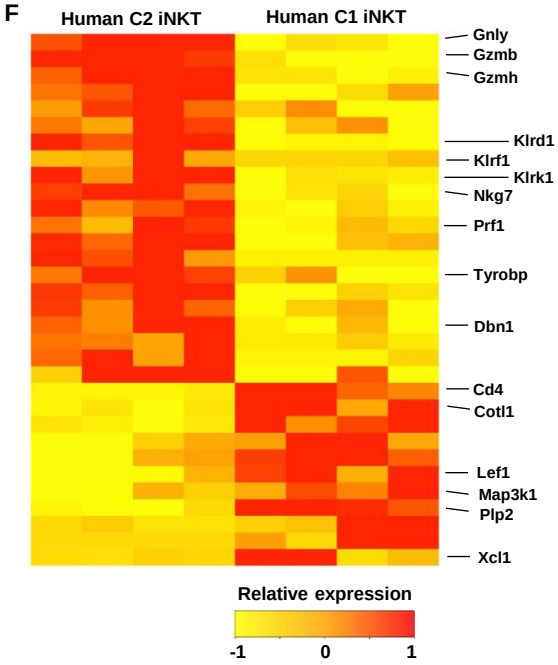

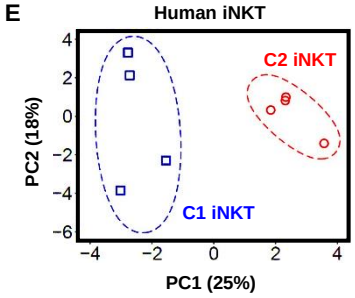

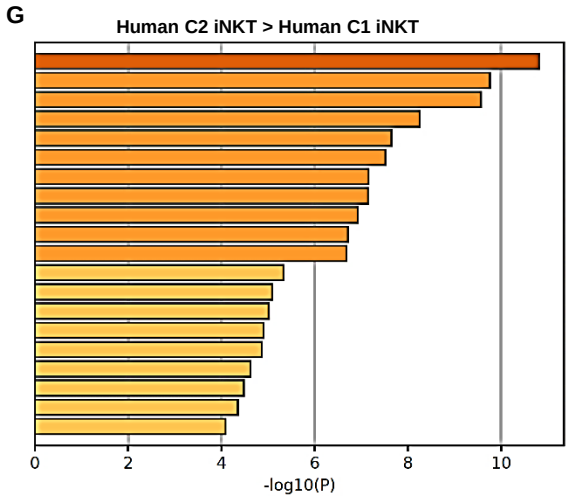

GO:0051249: Regulation of lymphocyte activation
WP5115: Network map of SRAS-CoV-2 signaling pathway
GO:0048534: Hematopoietic or lymphoid organ development
GO:0001819: Positive regulation of cytokine production
GO:0007167: Enzyme-linked receptor protein signaling pathway
GO:0001906: Cell killing
GO:0019835: Cytolysis
GO:0032814: Regulation of natural killer cell activation
GO:0006954: Inflammatory response
M288: Notch-mediated HES/HEY pathway
GO:1903706: Regulation of hemopoiesis
R-HAS-9012999: RHO-GTPase cycle
hsa05135: Yersinia infection
R-HAS-6798695: Neutrophil degranulation
GO:0001890: Placenta development
WP560: TGF-beta receptor signaling
GO:0071345: Cellular response to cytokine stimulation
GO:0009617: Response to bacterium
WP5218: Extrafollicular B cell activation by SARS-CoV-2
M195: C-MYB pathway

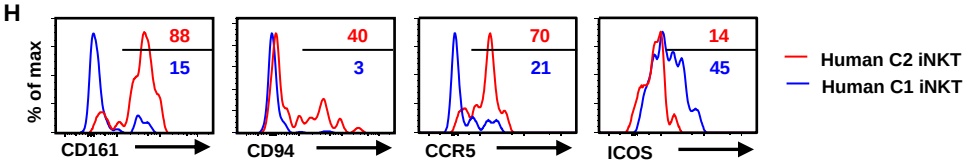

SUPPLEMENTARY MATERIALS

Supplementary Materials and Methods

Mice and generation of IL-15-floxed mice

IL-15-floxed mice were generated by targeting the insertion of the loxP sites into the endogenous IL-15 gene, as shown in fig. S2. To construct the targeting vector, we subcloned genomic DNA fragments encoding exons 3 to 6 of endogenous IL-15 gene from the C57BL/6 genome containing the 2.5-kb upstream and 6.0-kb downstream fragments of exon 5 by PCR. Two loxP sites were inserted 507 bp upstream and 243 bp downstream from the end of exon 5, respectively. The targeting construct was transfected by electroporation into the KY1.1 embryonic stem cell (ESC) line derived from C57BL/6J x 129S6/SvEvTac mouse embryos (a kind gift from Dr. J. Takeda, Osaka University), and targeted clones were screened by DTA/G418-resistance and PCR. Established ESC clones were injected into ICR eight-cell embryos to produce chimeric mice. Chimeric mice were bred with Flpe transgenic mice to remove the FRT-flanked neomycin resistance gene cassette (a kind gift of Dr. M. Mishina, Ritsumeikan University). IL-15-floxed mice were confirmed by PCR and DNA sequencing, backcrossed into C57BL/6 mice nine times, and then bred to Cre-driver mice to obtain conditional knockout strains.

SPC-Cre mice were obtained from Dr. Y. Oike and the Center for Animal Resources and Development (CARD), Kumamoto University. BALB/c mice were purchased from Japan SLC, and germ-free mice on a C57BL/6 background were purchased from CLEA Japan. IL-15Rα-floxed mice were purchased from the Jackson Laboratories.

Flow cytometry

Detailed antibody information is shown in Supplementary table S1. For intracellular staining, T cells were stained for surface antigens, fixed, permeabilized, and stained using the Foxp3 Staining Buffer Set or IC Fixation Buffer (Thermo Fisher Scientific). Cells were analyzed on a FACSVerse or a LSRFortessa X-20 flow cytometer (BD Biosciences) using FlowJo software. In the figures, values in gated areas indicate the percentages in each population.

Immunohistochemistry

For CD244 staining, thymic lobes were incubated overnight with biotin-labeled anti-CD244 antibody or isotype control. Then, the thymic lobes were washed and fixed with 4% paraformaldehyde for five hours and snap frozen. Tissue sections of 10 μm thickness were stained with anti-GFP, Alexa Flour 546-anti-rabbit IgG and FITC-anti-Aire (5H12) antibodies from Invitrogen, and DyLight488 anti-rabbit IgG (Poly4064), streptavidin-APC, FITC- or PE-anti-EpCAM (G8.8), and Brilliant Violet 421-anti-TCRβ (H57-589) antibodies from BioLegend. Confocal microscopy was performed with a TSC-SP8 microscope (Leica Microsystems).

Intrathymic injection

C0 iNKT cells were freshly isolated from 4-week-old CD45.1 mice, and 1.5×10^3 C0 iNKT cells in 10 μL PBS were injected into the thymus of CD45.2 recipient mice of the same age. Then, we analyzed $CD45.1^+$ thymocytes after enrichment by negative selection with MACS CD8 microbeads and LD columns (Miltenyi Biotec) 4 days after the injection.

Intravascular staining

Anti-CD45 antibody (3 μg/mouse, 30-F11, BioLegend) was administered intravenously 3 min before the isolation of lymphocytes from the lung. The frequency of $CD45^+$ intravascular cells and $CD45^-$ extravascular cells was calculated. For FTY720 treatment, mice were treated with 25 μg/mouse FTY720 (Calbiochem) injected intraperitoneally every day and assessed by intravascular staining with CD45 antibody on day 3.

In vivo stimulation of iNKT cells

Mice were administered with 1 μg/mouse α-galactosylceramide (α-Gal) every two days by intraperitoneal injection or with IL-15/IL-15Rα complex (RLI) (provided by Dr. J. M. Dijkstra) once a day by intravenous injection. Thymocytes were isolated and analyzed 4 days after the first administration. In the B16-F10 melanoma lung metastasis experiment, mice were administered intravenously 200 ng/mouse α-GalCer 2 days before the inoculation of B16-F10 melanoma cells as described previously (*33*). Then, the mice were intraperitoneally injected with 1 μg/mouse α-GalCer every two days. After 14 days, the lungs were checked for tumor metastasis.

Real-time RT-PCR

The results were analyzed by real-time RT-PCR using a StepOnePlus real time PCR system (Applied Biosystems) and normalized to the corresponding levels of *Hprt* mRNA in thymocyte cDNA from wild-type mice. The primer sequences were as follows: *Hprt*, 5'-GTTGGATACAGGCCAGACTTTGTTG-3' and 5'-GATTCAACTTGCGCTCATCTTAGGC-3'; *Ifng*, 5'-CTGCAGAGCCAGATTATCTC-3' and 5'-CATTGAATGCTTGGCGCTGG-3'; *Klf2*, 5'-GACCCACAAGTGGCACAA-3' and 5'-CTTTCGGTAGTGGCGGGTAA-3'; *Aire*, 5'-TGCATAGCATCCTGGACGGCTTCC-3' and 5'-CCTGGGCTGGAGACGCTCTTTGAG-3';

Ins2, 5'-GCGGCAAGACCTACACCAAG-3' and 5'-TCTACAATGCCACGCTTCT-3'; and *Fezf2*, 5'-ACCCAGCTTCCTATCCCCAT-3' and 5'-GAGCATTGAACACCTTGCCG-3'.

Bone marrow transplantation

Tie2-Cre IL-15 cKO host mice were irradiated with two separate doses of 4.5 Gy with a three-hour interval and injected intravenously with 5×10^5 bone marrow cells. After the transplantation, the mice were maintained on water containing antibiotics for about 2 weeks to prevent infection, and thymocytes were analyzed 5 weeks later.

Tumor inhibition assay

In vivo-pulsed effector cells (C2 iNKT, C1 iNKT, and NK cells) were isolated at day 4 from the lungs of wild-type mice inoculated with 1×10^5 B16-F10 tumor cells by intravenous injection and stimulated with 1 μg/mouse α-galactosylceramide (α-Gal) at day 0 and day 2 by intraperitoneal injection. For the target cell inhibition experiments, effector cells and 200 B16-F10 tumor target cells/well were seeded into 96-well round-bottom plates at the indicated effector to target ratios. Control wells were seeded with only 200 B16-F10 tumor target cells/well. After 10 hours incubation with 100 ng/ml IL-15 at 37℃ in 5% CO_2, each well was gently washed with PBS, and the remaining target cells were stained with trypan blue. The number of live target cells was counted, and the viability was calculated based on the number of live cells and normalized to that in control wells.

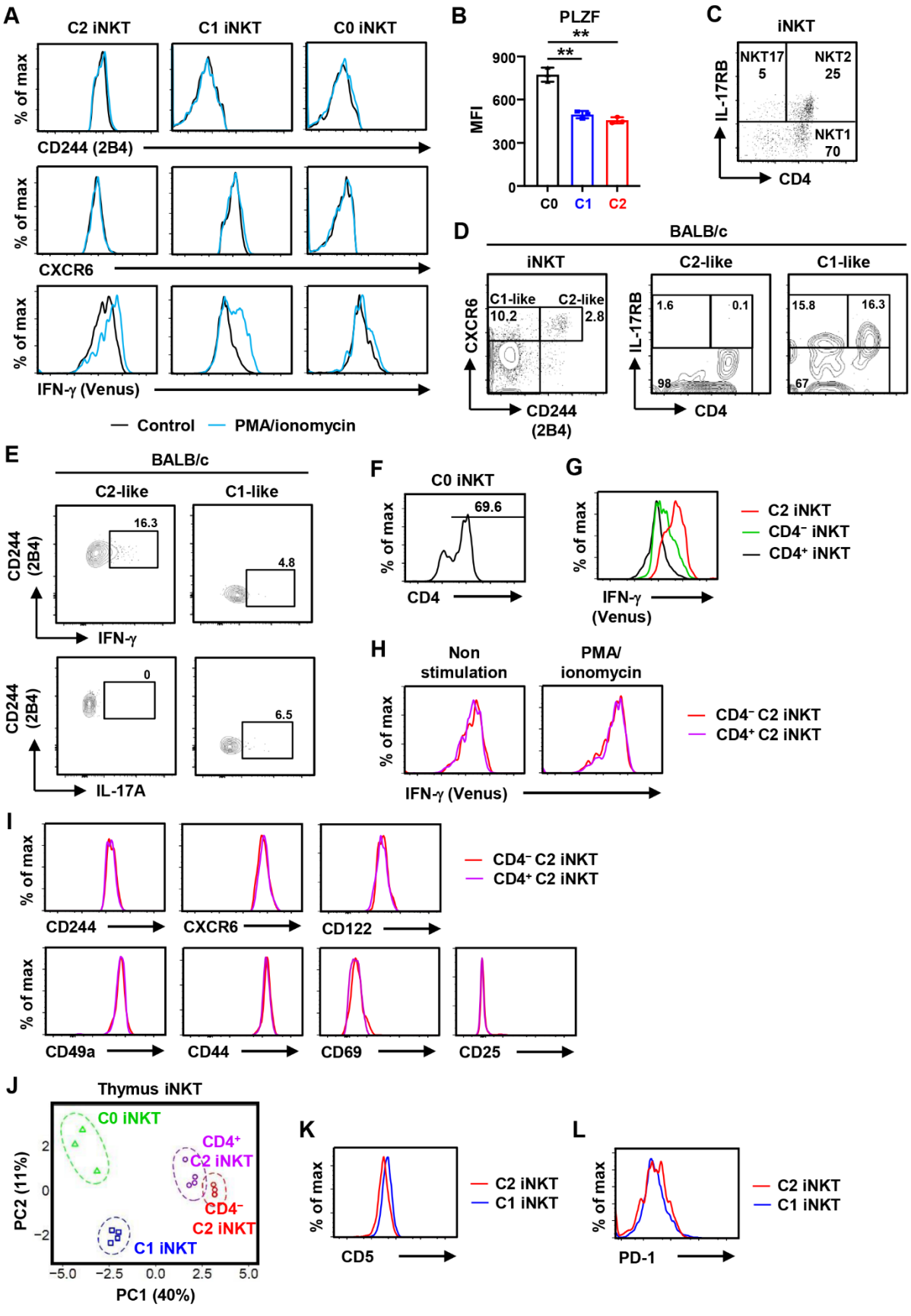

1

fig S1. Characterization of mouse C2 iNKT cells.

(A) Flow cytometric analysis of CD244, CXCR6, and IFN-γ expression in the indicated thymic iNKT cell subsets after stimulation with 25 ng/mL PMA and 1 μg/mL ionomycin for 4 hours. (**B**) The expression of PLZF in thymic iNKT cells presented as mean fluorescence intensity (MFI) (n = 3). **(C)** Gating strategy for NKT1, NKT2, and NKT17 cells in the thymus of C57BL/6 mice. **(D)** Flow cytometric analysis of C2- and C1-like iNKT cells in BABL/c mice. **(E)** Flow cytometric analysis of IFN-γ and IL-17A expression in C2- and C1-like iNKT cells from BALB/c mice after stimulation with PMA and ionomycin for 4 hours. **(F)** Flow cytometric analysis of CD4 expression in thymic C0 iNKT cells. **(G)** Flow cytometric analysis of IFN-γ expression in C2 iNKT cells, $CD4^+$ and $CD4^-$ iNKT cells. **(H)** Flow cytometric analysis of IFN-γ expression in $CD4^+$ and $CD4^-$ C2 iNKT cells with or without PMA and ionomycin stimulation for 4 hours. **(I)** Flow cytometric analysis of developmental and functional molecules in $CD4^+$ and $CD4^-$ C2 iNKT cells. **(J)** Principal component analysis (PCA) of $CD4^+$ and $CD4^-$ C2 iNKT cells. Expression data were measured by dRNA-seq from 3–4 biological replicates. **(K and L)** Flow cytometric analysis of CD5 (K) and PD-1 (L) in C2 and C1 iNKT cells. Data represent at least two independent experiments with similar results (A, C-I, K, and L). Data are mean ± SD pooled from two independent experiments (B); with Student's *t*-test. **, $p < 0.01$.

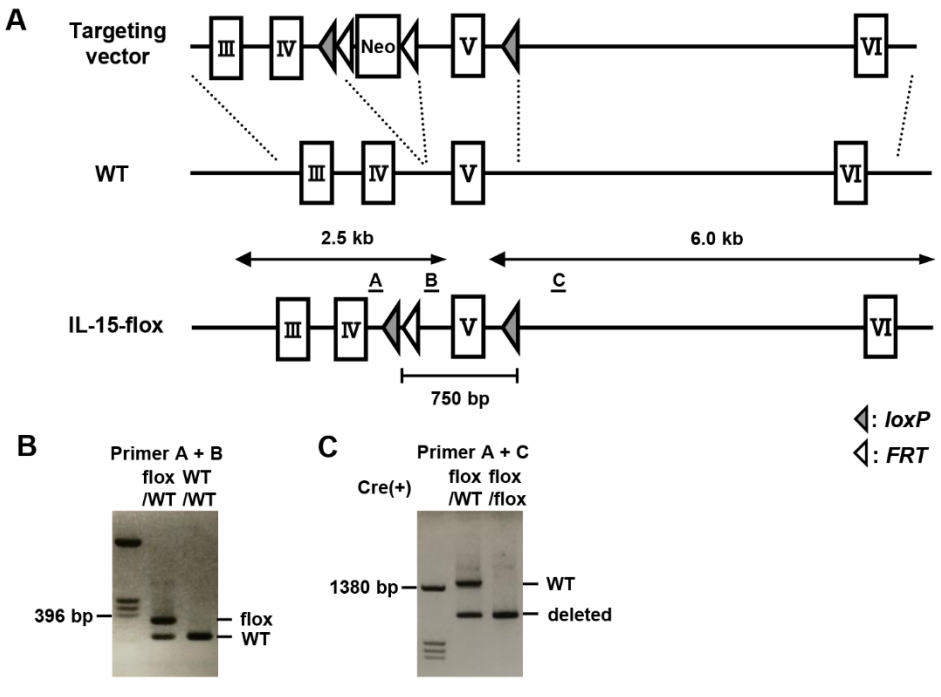

fig. S2. Generation of IL-15-floxed mice.

(A) Targeting strategy for the IL-15-floxed allele. Boxes indicate exons of the IL-15 locus. Gray and white triangles indicate loxP and FRT sequences, respectively. Horizontal bars indicate the primers for genotyping. The neomycin resistance gene cassette was excised by Flpe recombination. **(B)** Genotyping PCR to detect the IL-15-flox allele by the primers A and B shown in (A). **(C)** PCR analysis confirmed cKO in hematopoietic cells from Tie2-Cre; IL-15-flox/flox mice using the primers A and C shown in (A). Data represent at least four independent experiments with similar results (B and C).

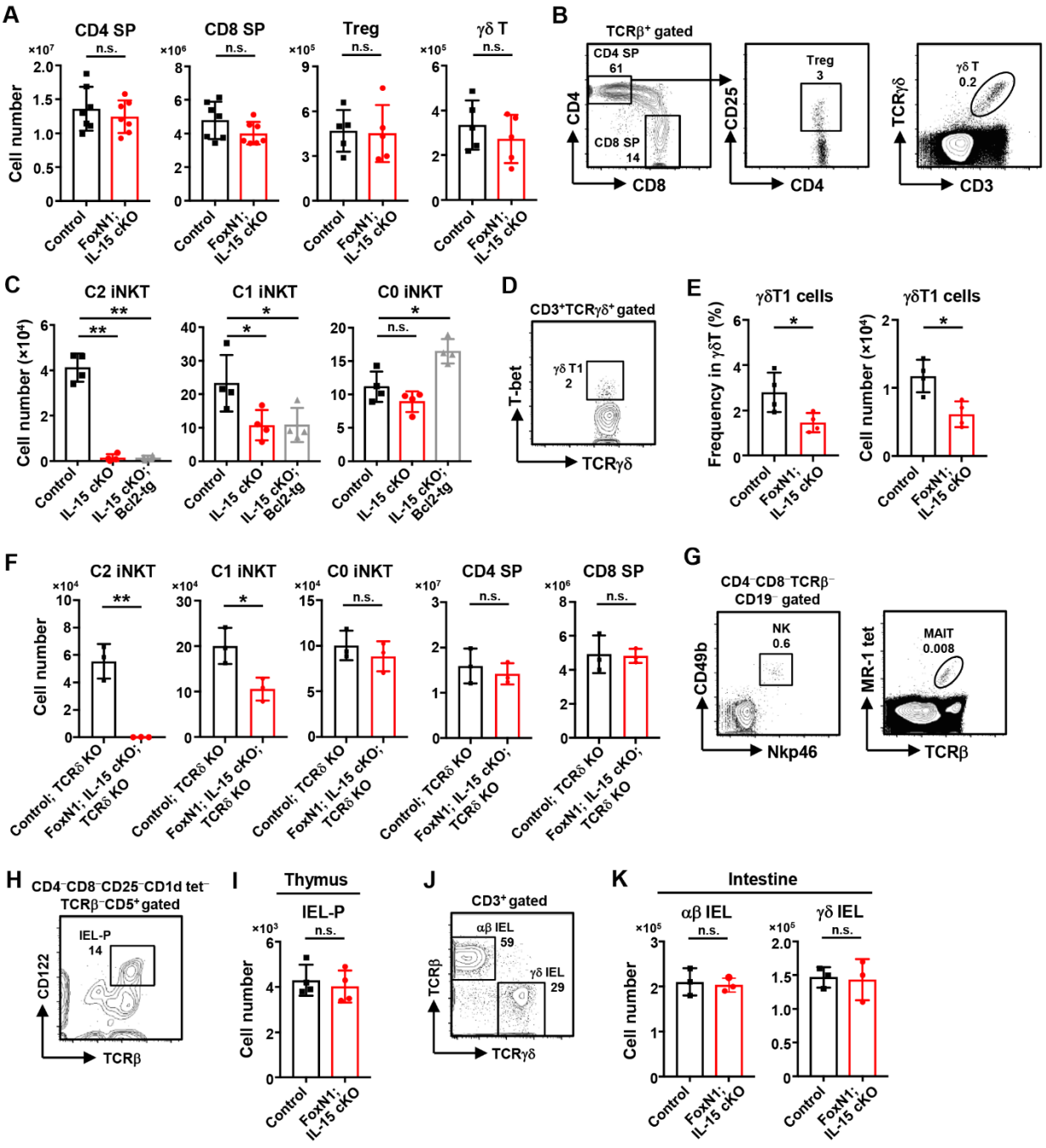

fig. S3. Effects of TEC-derived IL-15 on thymocytes.

(A) Number of indicated thymocytes in FoxN1-Cre IL-15 cKO (FoxN1; IL-15 cKO) mice and littermate control (Control) (n = 5–7). **(B)** Gating strategy for SP, Treg, and γδ T cells from the thymus. **(C)** Number of thymic C2, C1, and C0 iNKT cells in Bcl-2 transgenic (Bcl2-tg) FoxN1-

Cre IL-15 cKO mice (IL-15 cKO; Bcl2-tg), FoxN1-Cre IL-15 cKO mice (IL-15 cKO) and littermate control mice (n = 4). **(D)** Gating strategy for γδT1 cells from the thymus. **(E)** Frequency of γδT1 cells in γδ T cells and number of γδT1 cells in the thymus of FoxN1-Cre IL-15 cKO mice and littermate control (n = 4). **(F)** Number of indicated thymocytes in FoxN1-Cre IL-15 cKO × TCRδ KO mice (FoxN1; IL-15 cKO; TCRδ KO) and littermate control TCRδ KO mice (n = 3). **(G)** Gating strategy for NK and MAIT cells from the thymus. **(H and I)** Gating strategy (H) and number (I) of intraepithelial lymphocyte precursors (IEL-P) in the thymus of FoxN1-Cre IL-15 cKO mice and littermate control (n = 4). **(J and K)** Gating strategy (J) and number (K) of αβ and γδ intraepithelial lymphocytes (IELs) in the small intestine of FoxN1-Cre IL-15 cKO mice and littermate control (n = 3). Data are means ± SD and pooled from 2-4 independent experiments; Student's *t*-test or *t*-test with Welch's correction (A, E, F, I, and K) and with one-way ANOVA (C). **, $p < 0.01$; *, $p < 0.05$; n.s., not significant.

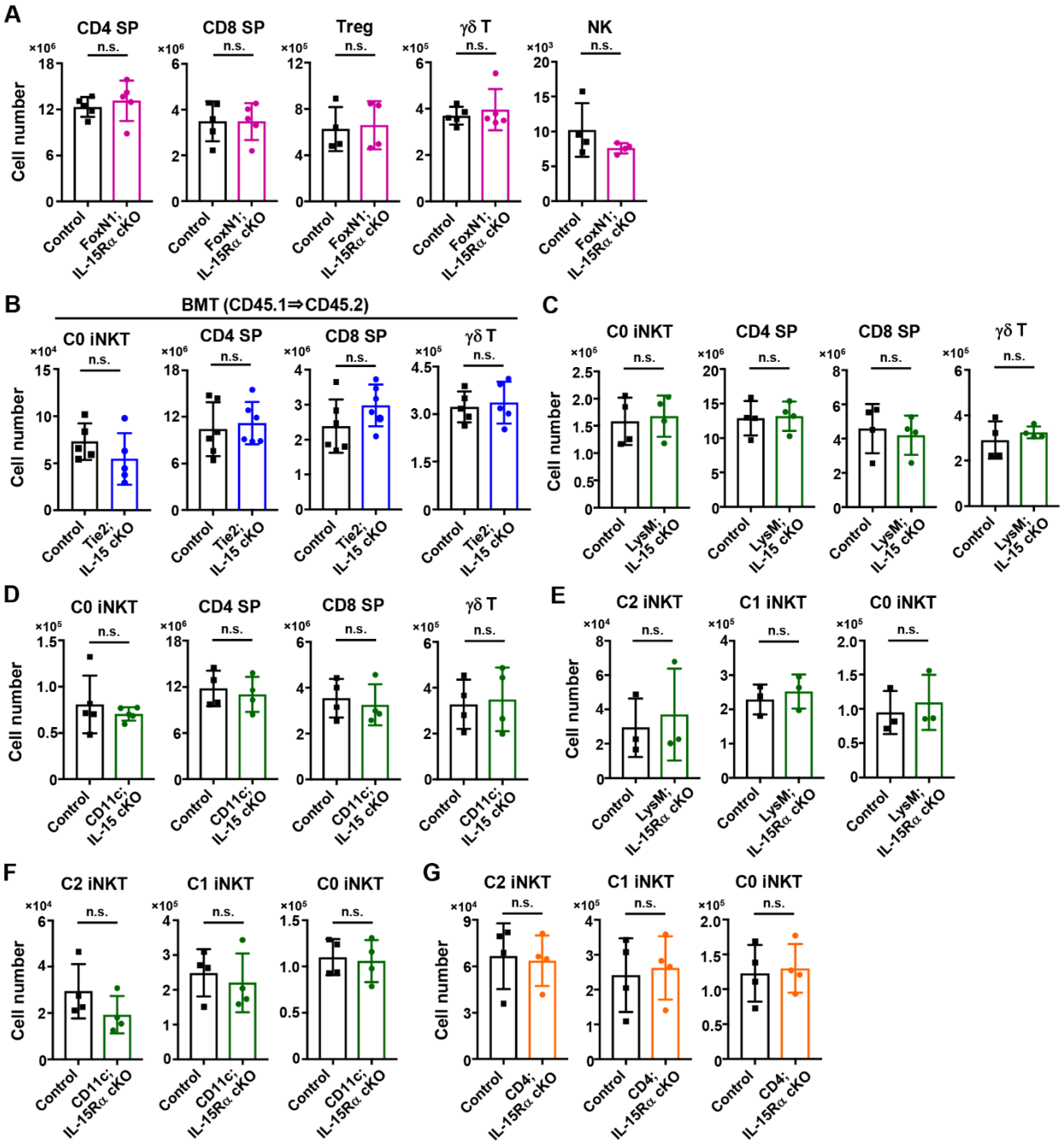

fig S4. IL-15 and IL-15Rα trans-presentation in thymocyte development.

(A) Number of indicated thymocytes in FoxN1-Cre IL-15Rα cKO mice (FoxN1; IL-15Rα cKO) and littermate control (Control) (n = 4–5). **(B)** Lethally irradiated hosts (Tie2-Cre IL-15 cKO mice and littermate control, CD45.2) were reconstituted with 1 × 10^6 bone marrow cells from wild-type mice (CD45.1). Number of indicated thymocytes in Tie2-Cre IL-15 cKO (Tie2; IL-15

cKO) or littermate control hosts 8 weeks after bone marrow transplantation (BMT) (n = 5–6). **(C and D)** Number of indicated thymocytes in LysM-Cre IL-15 cKO mice (LysM; IL-15 cKO) (C) (n = 4), CD11c-Cre IL-15 cKO mice (CD11c; IL-15 cKO) (D), and littermate control mice (n = 4–5). **(E and F)** Number of thymic C2, C1, and C0 iNKT cells in LysM-Cre IL-15Rα cKO mice (LysM; IL-15 Rα cKO) (E) (n = 3), CD11c-Cre IL-15Rα cKO mice (CD11c; IL-15 Rα cKO) (F) (n = 4), and littermate control mice. **(G)** Number of thymic C2, C1, and C0 iNKT cells in CD4-Cre IL-15Rα cKO mice (CD4; IL-15 Rα cKO) and littermate control mice (n = 4). Data are means ± SD and pooled from 2-4 independent experiments; Student's *t*-test. n.s., not significant.

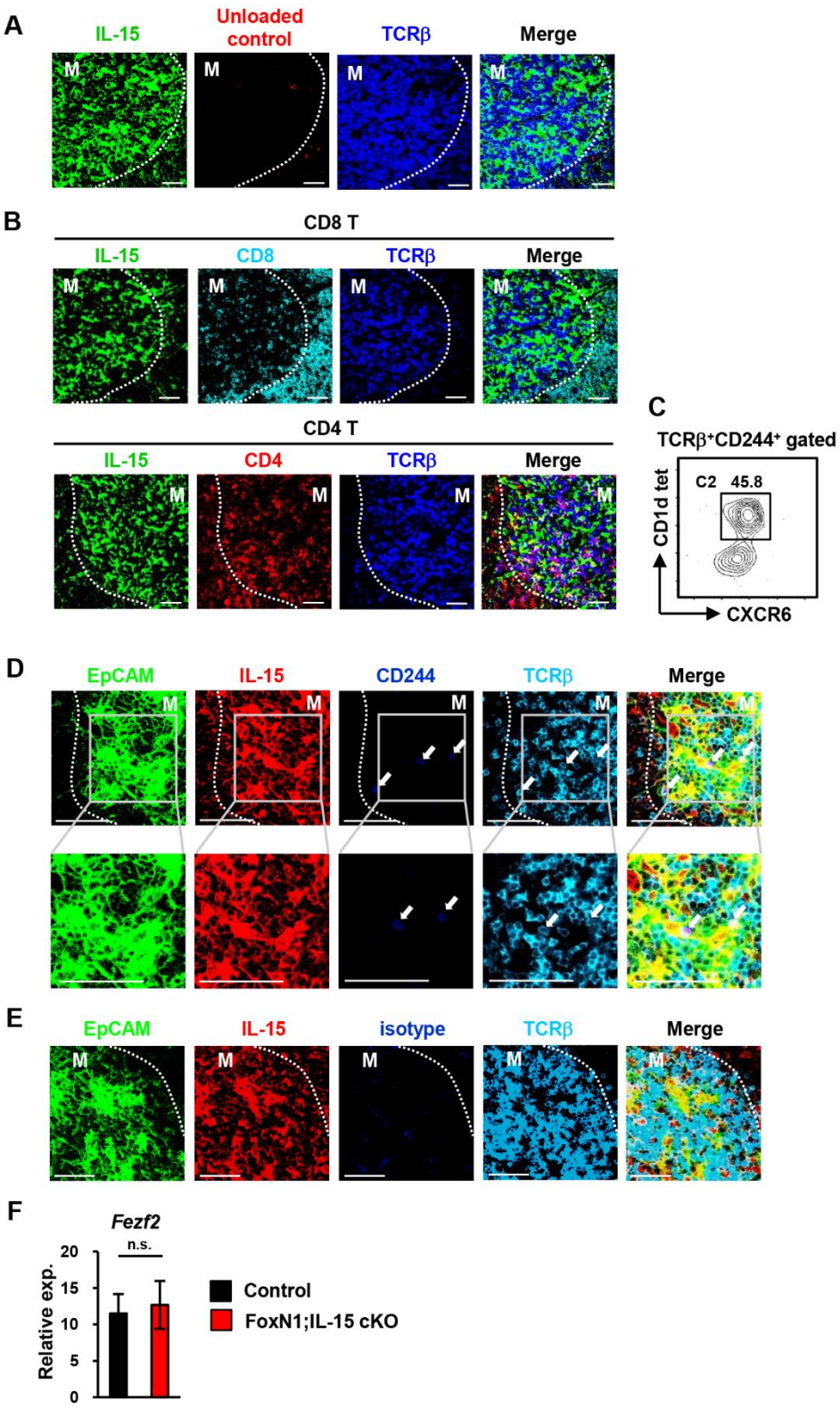

fig S5. Distribution of thymocytes and IL-15-producing mTECs in thymic medulla.

(A) Immunohistochemistry using PBS57-unloaded CD1d tetramer, the negative control for PBS57-loaded CD1d tetramer in Fig. 3E (n = 2). M, thymic medulla. Scale bars, 50 μm. **(B)** Immunohistochemistry for CD8 SP and CD4 SP cells in the thymus of IL-15-CFP knock-in mice (n = 3). M, thymic medulla. Scale bars, 50 μm. **(C)** Frequency of C2 iNKT cells in $TCR\beta^{+}CD244^{+}$ thymocytes. **(D)** Immunohistochemistry for $TCR\beta^{+}CD244^{+}$ cells in the thymus of IL-15-CFP knock-in mice. Boxed areas in the upper panels are enlarged in the lower panels (n = 3). M, thymic medulla. Scale bars, 50 μm. **(E)** Immunohistochemistry with isotype control for anti-CD244 antibody in (D) (n = 2). M, thymic medulla. Scale bars, 50 μm. **(F)** *Fezf2* mRNA levels relative to *Hprt* in freshly isolated mTECs from FoxN1-Cre IL-15 cKO mice or littermate control mice and measured by qPCR (n = 3). Data represent two (A and E) or three (B and D) separate mice with similar results. Data represent three independent experiments with similar results (C). Data are mean ± SEM (F) and pooled from three separate mice with duplicate measurement per mouse; Student's *t*-test. n.s., not significant.

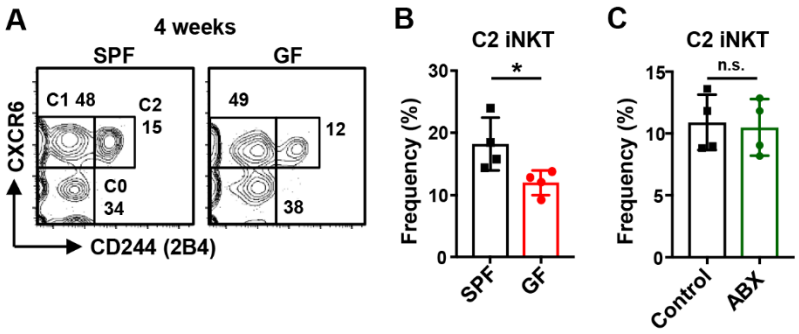

fig. S6. Effects of microbiome on C2 iNKT cells.

(A) Flow cytometric analysis of thymic iNKT cells in SPF and germ-free (GF) mice. **(B)** Frequency of thymic C2 iNKT cells in the mature NK1.1^{+} iNKT population shown in (A) (n = 4). **(C)** Eight-week-old wild-type mice were fed antibiotics-containing water or control water for 4 weeks. Frequency of thymic C2 iNKT cells in the mature iNKT population of antibiotic-treated (ABX) and control 12-week-old mice (n = 4). Data represent two independent experiments with similar results (A). Data are means ± SD and pooled from two independent experiments (B and C); Student's *t*-test. *, $p < 0.05$; n.s., not significant.

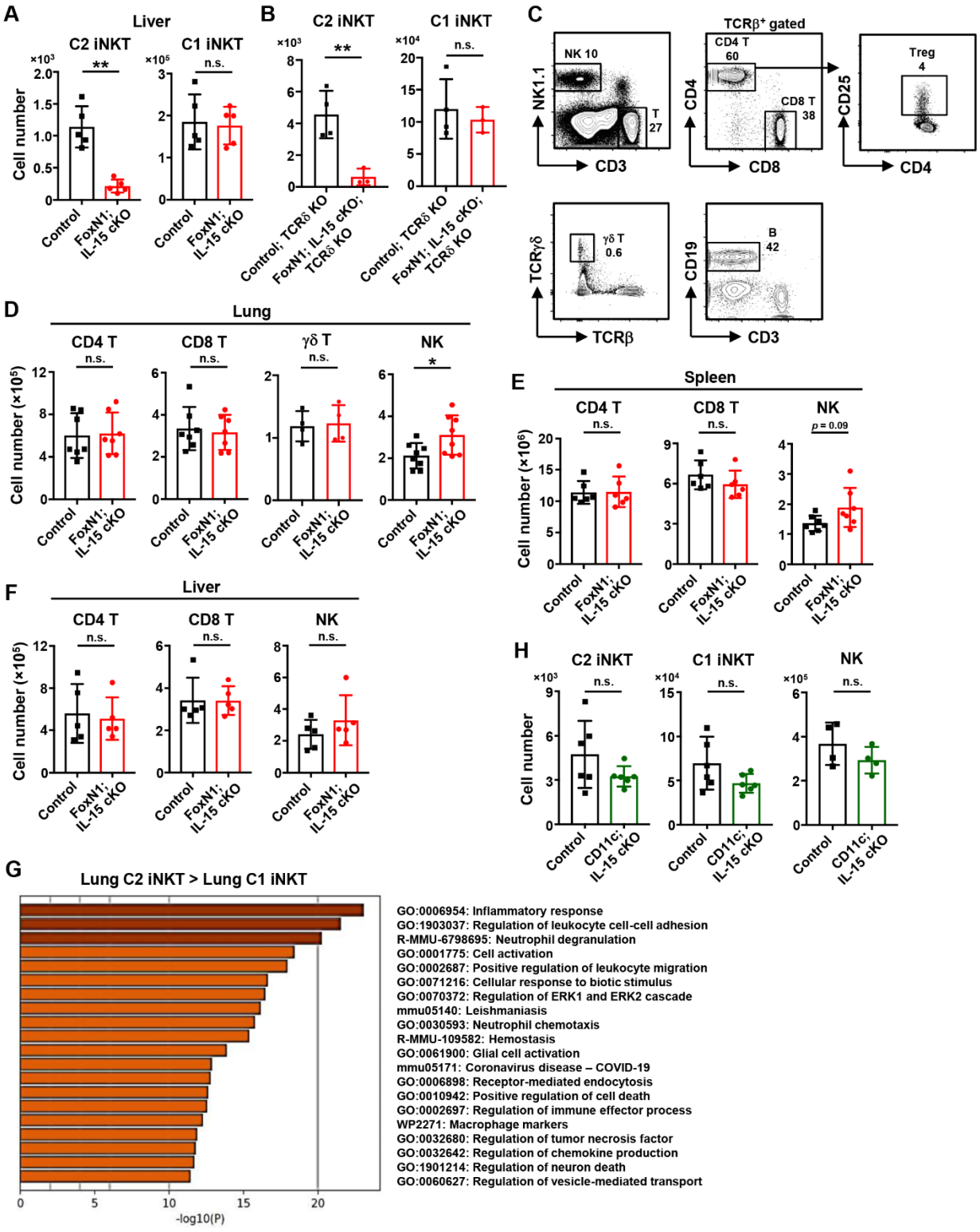

GO:0006954: Inflammatory response
GO:1903037: Regulation of leukocyte cell-cell adhesion
R-MMU-6798695: Neutrophil degranulation
GO:0001775: Cell activation
GO:0002687: Positive regulation of leukocyte migration
GO:0071216: Cellular response to biotic stimulus
GO:0070372: Regulation of ERK1 and ERK2 cascade
mmu05140: Leishmaniasis
GO:0030593: Neutrophil chemotaxis
R-MMU-109582: Hemostasis
GO:0061900: Glial cell activation
mmu05171: Coronavirus disease – COVID-19
GO:0006898: Receptor-mediated endocytosis
GO:0010942: Positive regulation of cell death
GO:0002697: Regulation of immune effector process
WP2271: Macrophage markers
GO:0032680: Regulation of tumor necrosis factor
GO:0032642: Regulation of chemokine production
GO:1901214: Regulation of neuron death
GO:0060627: Regulation of vesicle-mediated transport

fig. S7. iNKT cells and relevant lymphocytes in peripheral tissues of IL-15 cKO mice.

(A) Number of liver iNKT cells in FoxN1-Cre IL-15 cKO mice (FoxN1; IL-15 cKO) and littermate control mice (Control) (n = 5). **(B)** Number of iNKT cells in the lung of FoxN1-Cre IL-15 cKO × TCRδ KO mice (FoxN1; IL-15 cKO; TCRδ KO) and control TCRδ KO mice (n = 3–4). **(C)** Gating strategy for the indicated lymphocytes from the lung. **(D to F)** Number of indicated lymphocytes in the lung (D) (n = 4–8), spleen (E) (n = 6–7) and liver (F) (n = 5) of FoxN1-Cre IL-15 cKO mice and littermate control mice. **(G)** Bar chart depicting the functional analysis of differentially expressed genes between lung C2 and C1 iNKT cells. Normalized enrichment scores were calculated using Metascape. **(H)** Number of indicated lung lymphocytes in CD11c-Cre IL-15 cKO mice (CD11c; IL-15 cKO) (n = 4–6). Data are means ± SD and pooled from 2-5 independent experiments (A, B, D, E, F, and H); Student's *t*-test. **, $p < 0.01$; *, $p < 0.05$; n.s., not significant.

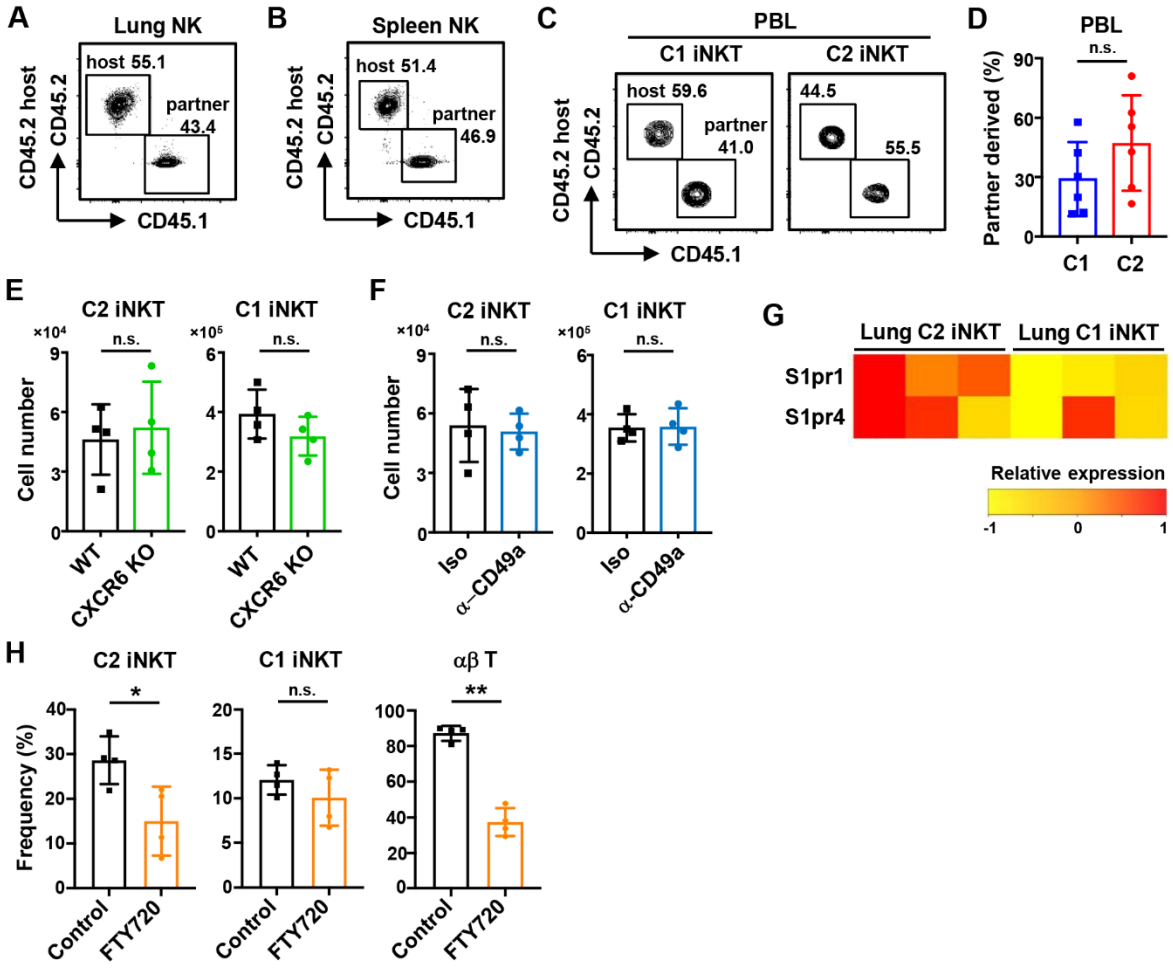

fig. S8. Circulation and retention of iNKT cells and NK cells.

(A and B) Genetically marked CD45.1 and CD45.2 mice of the same age underwent parabiosis surgery and were analyzed 60 days later. Flow cytometric analysis for partner-derived and host-derived NK cells in the lung (A) or spleen (B) (n = 6). **(C and D)** Flow cytometric analysis of partner-derived and host-derived C2 and C1 iNKT cells among peripheral blood lymphocytes (PBL) after parabiosis surgery (C). Frequency of partner-derived C2 and C1 iNKT cells of PBL (D) (n = 6). **(E)** Number of thymic C2 and C1 iNKT cells in CXCR6-GFP/GFP mice (CXCR6 KO) and wild-type (WT) mice (n = 4). **(F)** WT mice were administered anti-integrin α1 (α-CD49a) blocking antibody or isotype control (Iso) by intravenous injection every two days. Number of thymic C2 and C1 iNKT cells 6 days after the first antibody administration (n = 4).

(G) Expression of S1pr1 and S1pr4 in C2 and C1 iNKT cells measured by dRNA-seq from three biological replicates. **(H)** WT mice were administered FTY720 by intraperitoneal injection for three days. Frequency of $CD45^+$ intravascular cells among the indicated lymphocytes by the intravascular staining of CD45 (n = 4). Data represent three independent experiments with similar results (A to C). Data are means ± SD and pooled from 2-3 independent experiments (D-F and H); Student's *t*-test. **, $p < 0.01$; *, $p < 0.05$; n.s., not significant.

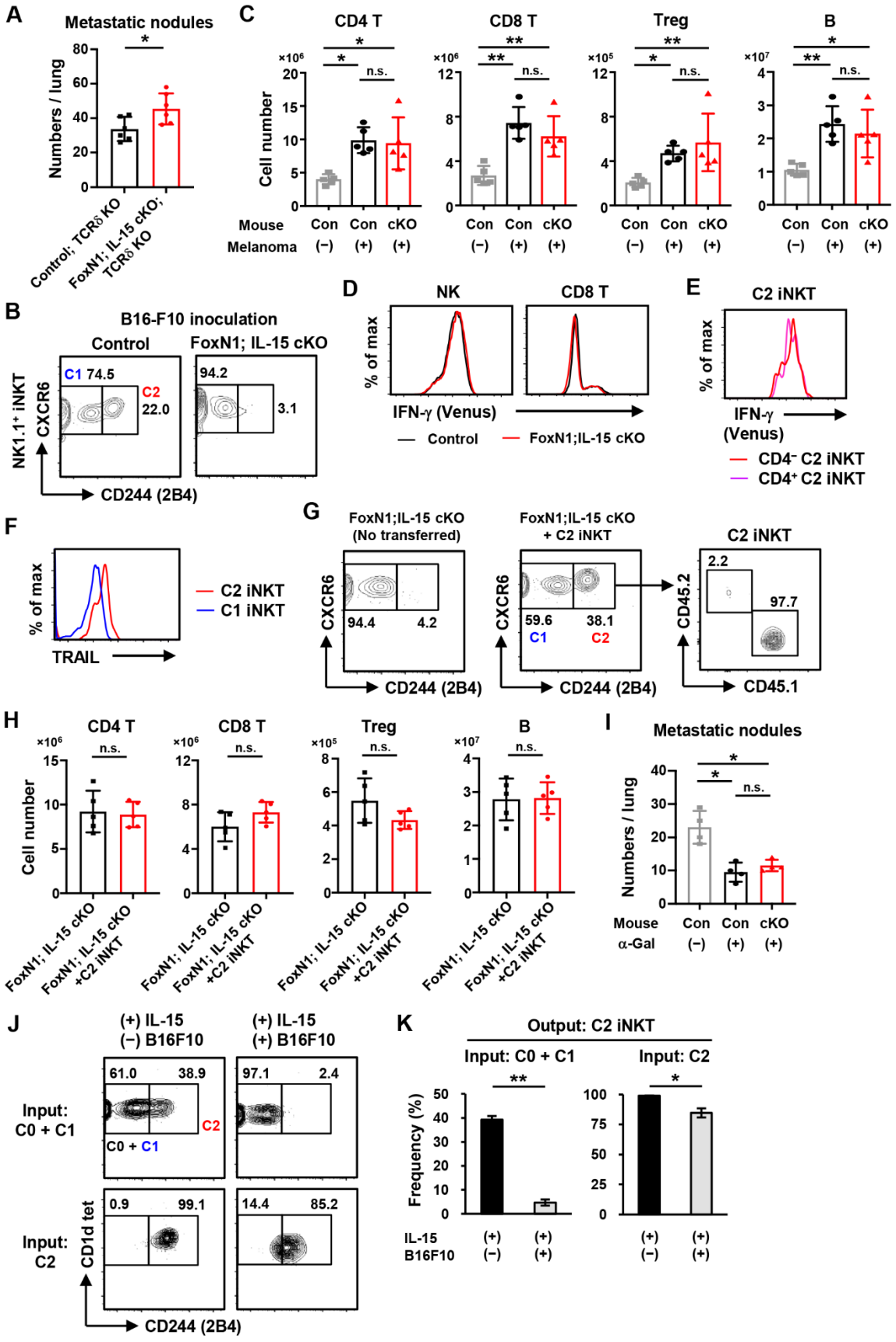

1

fig. S9. Alterations of relevant lymphocytes in a B16-F10 melanoma cell metastasis model.

(A) Mice were intravenously injected with 4×10^4 B16-F10 melanoma cells, and the number of metastatic nodules in the lung of FoxN1-Cre IL-15 cKO × TCRδ KO mice (FoxN1; IL-15 cKO; TCRδ KO) or littermate control TCRδ KO mice after 14 days of inoculation is shown (n = 6). **(B)** Flow cytometric analysis of C1 and C2 iNKT cells in the lung 14 days after the inoculation. **(C)** FoxN1-Cre IL-15 cKO (cKO) mice or littermate control mice (Con) were administered (+) or without (−) 4×10^4 B16-F10 melanoma cells 14 days before the analysis. Number of indicated lymphocytes in the lung is shown (n = 5). **(D and E)** Flow cytometric analysis of IFN-γ expression in NK cells and CD8 T cells (D) and C2 iNKT cells (E) in the lung of FoxN1-Cre IL-15 cKO × IFN-γ-Venus reporter mice and control IFN-γ-Venus reporter mice 14 days after the inoculation of melanoma cells. **(F)** Flow cytometric analysis for TRAIL expression in iNKT cells after culture with B16-F10 melanoma cells in the presence of IL-15. **(G)** CD45.1 C2 iNKT cells were adoptively transferred into CD45.2 FoxN1-Cre IL-15 cKO mice. Flow cytometric analysis of transferred CD45.2 C2 iNKT cells in the lung of recipients 4 days after the inoculation of melanoma cells. **(H)** Number of indicated relevant lymphocytes 14 days after the inoculation of melanoma cells in CD45.2 FoxN1-Cre IL-15 cKO recipients with or without the adoptive transfer of CD45.1 C2 iNKT cells (n = 5). **(I)** FoxN1-Cre IL-15 cKO mice (cKO) and littermate control mice (Con) were administered α-galactosylceramide (α-Gal) (+) or control PBS (−). The number of metastatic nodules in the lung of the indicated mice 14 days after the inoculation of melanoma cells (n = 4). **(J)** Flow cytometric analysis of C2 and C0+C1 thymic iNKT cells after 4 days of culture with or without B16-F10 melanoma cells in the presence of IL-15. **(K)** Frequency of the C2 iNKT cells shown in (J) (n = 3). Data are means ± SD and pooled from 2-3 independent experiments; Student's *t*-test (A, H and K) and one-way ANOVA (C and I). Data

represent at least three independent experiments with similar results (B, D-G, and J). **, $p < 0.01$; *, $p < 0.05$; n.s., not significant.

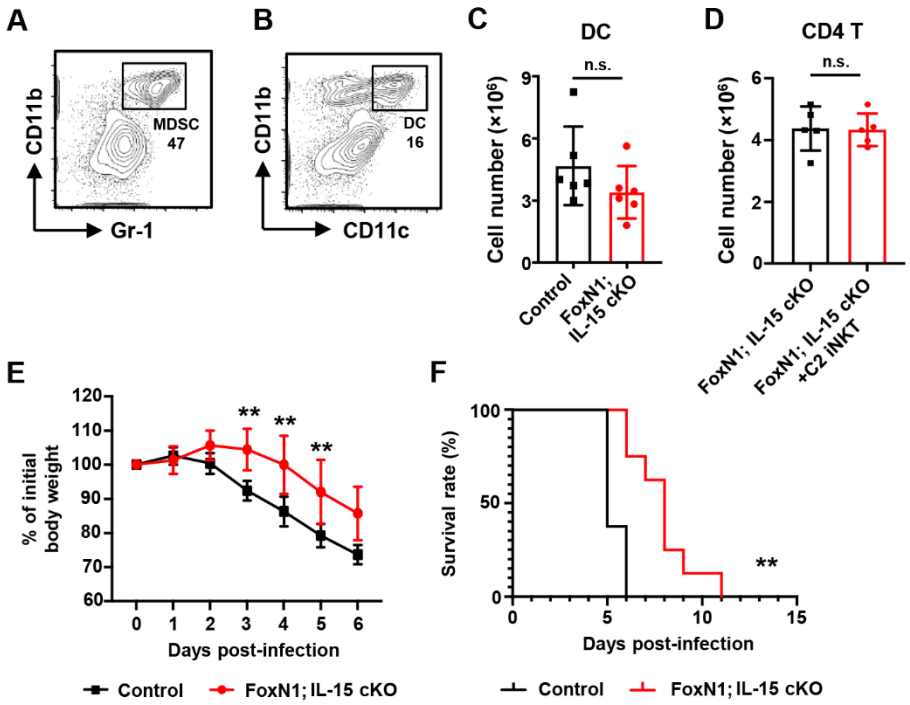

fig. S10. Alterations of relevant lymphocytes in an influenza virus infection model.

(A) Gating strategy for myeloid-derived suppressor cells (MDSCs) in the lung of mice on day 7 post infection by 0.5 LD_{50} of influenza A virus (IAV). **(B and C)** Gating strategy (B) and number (C) of DCs in the lung of FoxN1-Cre IL-15 cKO and control mice on day 7 post infection (n = 6). **(D)** Number of CD4 T cells in the lung of FoxN1-Cre IL-15 cKO mice with or without the adoptive transfer of C2 iNKT cells on day 7 post infection (n = 5). **(E)** Body weight changes of age-matched FoxN1-Cre IL-15 cKO and control mice at the early phase post inoculation with a lethal dose (2 LD_{50}) of IAV. Each group consists of 8 female mice. **(F)** Survival rate of age-matched FoxN1-Cre IL-15 cKO and control mice following intranasal infection with IAV at the lethal dose (2 LD_{50}). Mice were monitored daily until death occurred or euthanized in case of greater than 20% weight loss. Each group consists of 8 female mice, and the difference was evaluated by the log rank test. Data are means ± SD (C. D, and E) and pooled from 2-4 independent experiments; Student's t-test. **, $p < 0.01$; n.s., not significant.

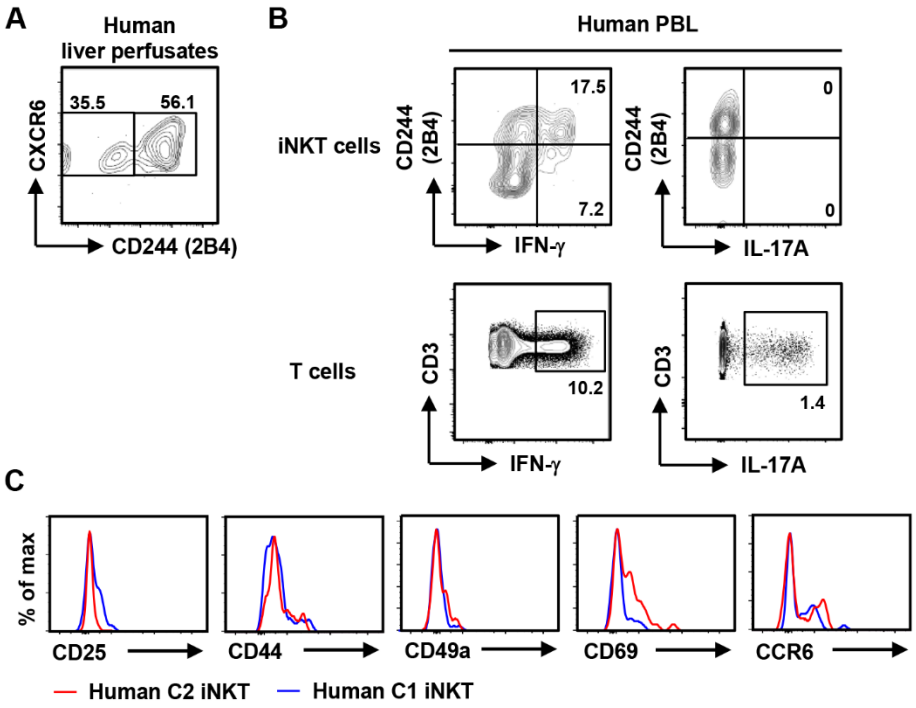

fig. S11. Characterization of human iNKT cells.

(A) Flow cytometric analysis of human C1 ($CD244^{-}CXCR6^{+}$) and C2 ($CD244^{+}CXCR6^{+}$) iNKT cells in liver perfusates. **(B)** Flow cytometric analysis of IFN-γ and IL-17A expression in human T cells, C1, and C2 iNKT cells after stimulation with 25 ng/mL PMA and 1 μg/mL ionomycin for 4 hours. **(C)** Flow cytometric analysis of developmental and functional molecules in human C1 and C2 iNKT cells. Data represent at least two independent experiments with similar results (A-C).

Table S1. List of antibodies used for flow cytometry

Mouse

Antibody	Fluorescence	Clone	Company	Catalog number	RRID
TCRβ	FITC	H57-597	BioLegend	109206	AB_313429
TCRβ	PE	H57-597	BioLegend	109208	AB_313431
TCRβ	APC	H57-597	BioLegend	109211	AB_313434
TCRβ	APC/Cy7	H57-597	BioLegend	109219	AB_893626
TCRβ	Brilliant Violet 421	H57-597	BioLegend	109230	AB_2562562
CD3ε	FITC	145-2C11	BioLegend	100306	AB_312671
CD3ε	PE/Cy7	145-2C11	Thermo Fisher Scientific	25-0031-82	AB_469572
CD4	APC-eFluor 780	RM4.5	Thermo Fisher Scientific	47-0042-82	AB_1272183
CD5	FITC	53-7.3	BioLegend	100605	AB_312734
CD8α	eFluor 450	53-6.7	Thermo Fisher Scientific	48-0081-82	AB_1272198
CD8α	PE/Cy7	53-6.7	TONBO	60-0081	AB_2621832
CD11b	APC/Cy7	M1/70	BioLegend	101225	AB_830641
CD11c	PE/Cy7	N418	BioLegend	117318	AB_493568
CD25	FITC	PC61	BioLegend	102005	AB_312854
CD44	PE/Cy7	IM7	Thermo Fisher Scientific	25-0441-82	AB_469623
CD49a	PE	Ha31/8	BD Bioscience	562115	AB_11153117
CD49a	Brilliant Violet 421	Ha31/8	BD Bioscience	740046	AB_2739815
CD49b	Pacific Blue	DX5	BioLegend	108918	AB_2265144
CD69	PE/Cy7	H1.2F3	Thermo Fisher Scientific	25-0691-82	AB_469637
CD45	APC/Cy7	30-F11	BioLegend	103115	AB_312980
CD45.1	Brilliant Violet 510	A20	BioLegend	110741	AB_2563378
CD45.2	FITC	104	Thermo Fisher Scientific	11-0454-82	AB_465061
CD122	Biotin	TM-β1	BioLegend	123205	AB_940607
CD244.1	APC	C9.1	Thermo Fisher Scientific	17-2440-82	AB_2573188
CD244.2	Alexa Fluor 647	m2B4(B6)458.1	BioLegend	133509	AB_2072854
CD244.2	PE/Cy7	m2B4(B6)458.1	BioLegend	133511	AB_2564338
CD244.2	Biotin	m2B4(B6)458.1	BioLegend	133505	AB_1626229
CD244.2	Biotin	2B4	BD Bioscience	557452	AB_396714
NK1.1	PE	PK136	BioLegend	108708	AB_313395
NK1.1	APC	PK136	BioLegend	108709	AB_313396

TCRγδ	APC	GL3	BioLegend	118116	AB_1731813
TCRγδ	PE/Cy7	GL3	BioLegend	118124	AB_11204423
CXCR6	FITC	SA051D1	BioLegend	151107	AB_2572144
CXCR6	APC	SA051D1	BioLegend	151105	AB_2572142
TRAIL	PE	N2B2	BioLegend	109305	AB_2303575
KLRG1	APC/Cy7	2F1	BioLegend	138425	AB_2566553
IFN-γ	FITC	XMG1.2	Thermo Fisher Scientific	11-7311-82	AB_465412
IFN-γ	PE/Cy7	XMG1.2	BioLegend	505826	AB_2295770
IL-17A	PE/Cy7	eBio17B7	Thermo Fisher Scientific	25-7177-82	AB_10732356
IL-17RB	eFluor 660	MUNC33	Thermo Fisher Scientific	12-7361-82	AB_2572658
PD-1	APC	29F.1A12	BioLegend	135209	AB_2251944
ICOS	PE	C398.4A	Thermo Fisher Scientific	12-9949-81	AB_466277
P2X7R	PE	1F11	BioLegend	148703	AB_2650951
Gr-1	FITC	RB6-8C5	BioLegend	108406	AB_313371
F4/80	PE	BM8	BioLegend	123109	AB_893498
EpCAM	FITC	G8.8	BioLegend	118207	AB_1134106
Ly-51	Alexa Fluor 647	6C3	BioLegend	108311	AB_2099614
Bcl-2	PE	BCL/10C4	BioLegend	633507	AB_2043939
Bcl-X	PE	7B2.5	GeneTex	GTX46035	AB_774264
Ki-67	PE	SolA15	Thermo Fisher Scientific	12-5698-82	AB_11150954
PLZF	PE	9E12	BioLegend	145803	AB_2561966
T-bet	PE	4B10	Thermo Fisher Scientific	12-5825-82	AB_925761
Granzyme B	eFluor 660	NGZB	Thermo Fisher Scientific	50-8898-82	AB_11219679
Perforin	APC	S16009B	BioLegend	154403	AB_2721464

Human

Antibody	**Fluorescence**	**Clone**	**Company**	**Catalog number**	**RRID**
CD3	APC	UCHT1	BioLegend	300458	AB_2564151
CD4	APC/Cy7	RPA-T4	BioLegend	300518	AB_314086
CD25	PE	BC96	BioLegend	302606	AB_314276
CD44	PE	IM7	BioLegend	103008	AB_312959
CD49a	PE	TS2/7	BioLegend	328303	AB_1236441
CD69	PE	FN50	BioLegend	310905	AB_314840
CD94	PE	DX22	BioLegend	305506	AB_314536
CD161	PE	HP-3G10	BioLegend	339903	AB_1501086
CD244	PE/Cy7	C1.7	BioLegend	329520	AB_2572017
CXCR6	FITC	K041E5	BioLegend	356020	AB_2715815

CCR5	PE	2D7	BD Bioscience	555993	AB_396279
CCR6	PE	11A9	BD Bioscience	559562	AB_397273
ICOS	PE	C398.4A	Thermo Fisher Scientific	12-9949-81	AB_466277
IFN-γ	PE	4S.B3	BioLegend	502508	AB_315233
IL-17A	PE	BL168	BioLegend	512305	AB_961395

1